Translocation of a vesicle through a narrow pore

PhD Thesis

Translocation of a vesicle through a narrow pore
(ベシクルの細孔透過過程)

Petch Khunpetch

Department of Physics
Graduate School of Science
Tohoku University

September, 2018

Translocation of a vesicle through a narrow pore

Theoretical Condensed Matter and Statistical Physics Group
Department of Physics, Graduate School of Science, Tohoku University
Petch Khunpetch

I. INTRODUCTION

Vesicles are considered as one of the main components of life. They consist of a bilayer membrane of amphiphilic molecules that are composed of a "water-loving (polar)" head-group and a "water-avoiding" hydrocarbon chains. Even though the membrane of vesicle has a thickness of typically a few nanometers, the size of vesicle can be in the order of up to 100 micrometers. Lipid bilayer vesicles are remarkably flexible surfaces that show a wide variety of shape deformation due to external conditions.

The dynamical aspect of vesicles, especially, the translocation through a narrow pore due to external driving forces is an interesting problem. The mechanism is relevant to, for example, many transdermal applications, transendothelial migration in immune system and drug delivery in pharmacological research etc. The interesting question is that how the effectiveness of such filtration process depends on various parameters of the system such as the driving forces, bending and stretching moduli of the vesicle, the initial size of the vesicle, and geometry and size of the pore.

In this research, we use Onsager variational principle to study translocation phenomena of a vesicle through a pore. We are interested in two problems of such a kind of this translocation process. First, we investigate translocation process of a vesicle through a hole in a solid membrane separating two chambers, where we focus on the kinetic pathway of the translocation. Onsager principle can give us the kinetic pathways of the state changes. On the other hand, the minimum energy paths or the reaction paths can be obtained by employing the string method. Our main purpose is to discuss the paths obtained from these two different methods when the external driving force changes. The second problem is the birthing of a vesicle through a small pore in self-reproducing vesicle system. The binary giant unilamellar vesicle (GUV) constituted of cylinder- and inverse-cone-surfactants can form an inclusion vesicle, called the daughter vesicle inside the mother vesicle and then the inclusion vesicle is expelled through the pore by a controlled temperature cycling. We again use the Onsager principle to investigate the birthing process of the daughter vesicle.

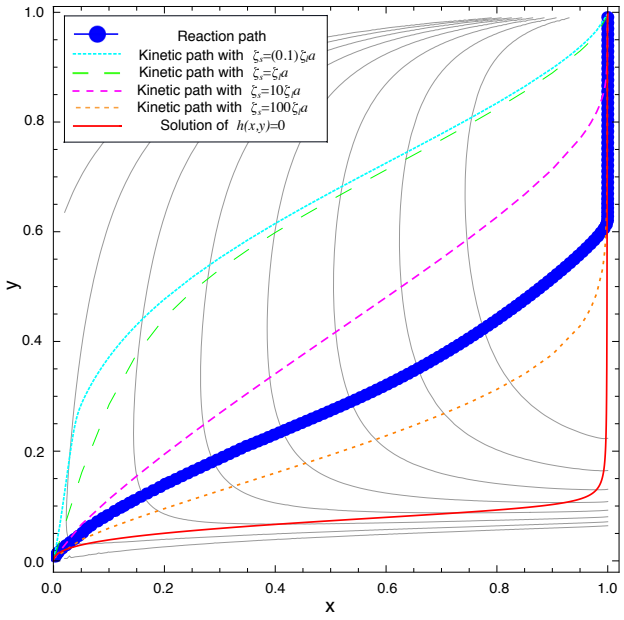

FIG. 1. The reaction and the kinetic paths at large pressure difference $\Delta Pa = \lambda$.

II. TRANSLOCATION OF A VESICLE THROUGH A NARROW HOLE ACROSS A MEMBRANE [1]

We simply model a translocating vesicle by two connected spheres. Due to the pressure difference across the membrane, the vesicle can translocate through the pore from one side to another side.

At large pressure difference $\Delta Pa = \lambda$, where a and λ are the radius of the hole and the stretching modulus, respectively, Fig. 1 shows the difference between the reaction path (blue line with filled circle) obtained from the string method and the kinetic paths obtained from the Onsager principle when the friction parameter changes. Figure 1 indicates that reaction and kinetic paths are significantly different from each other if the external force is large. Because the external force exerted on the liquid flow induces a quick flow of the liquid compared to the diffusion of the surfactant molecules, the time evolution of x (liquid volume) is much faster than the evolution of y (number of the surfactant molecules). This is why we have the difference between the result from the string method and the kinetic paths obtained from the Onsager principle. The solid red line indicates the kinetic path for large value of the friction coefficient of the hole on the surfactant molecules ζ_s.

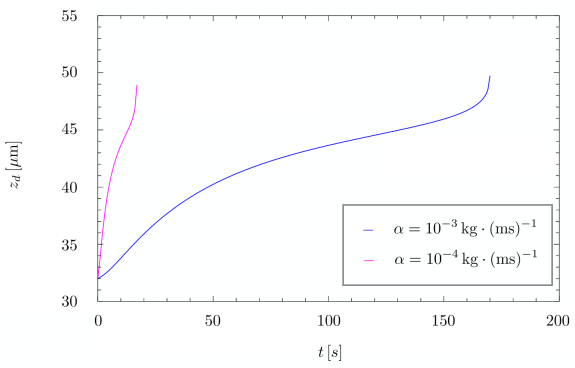

FIG. 2. The motion of the daughter vesicle with different value of the friction coefficient.

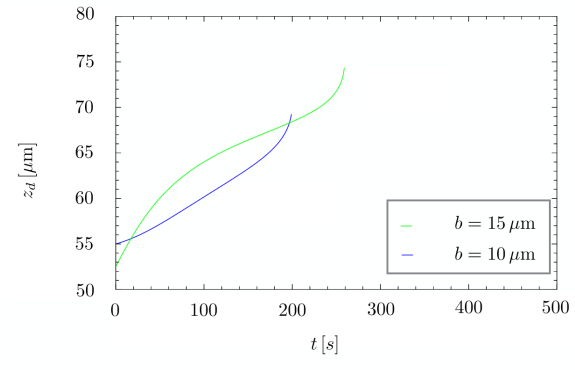

FIG. 3. The trajectory of the daughter vesicle with different size b.

Moreover, we see clearly that the translocation time decreases when the pressure difference increases and, at the same value of the pressure difference, the vesicle has succeeded in the translocating with less translocation time for the small value of ζ_s. Our results also suggest that the translocation time increases as the initial size of the vesicle increases at a given value of the pressure difference.

III. BIRTHING OF A DAUGHTER VESICLE IN SELF-REPRODUCING VESICLE SYSTEM

In this problem, we present theoretical model on the birthing process of a single, rigid daughter vesicle through a pore by using a simple geometric ansatz. By solving the equation of motion of the daughter vesicle derived by using Onsager principle numerically, we obtain the trajectory of the daughter vesicle when the friction coefficient changes as shown in Fig. 2. The results show clearly that the translocation time decreases when the friction caused by the pore against the motion of the daughter vesicle decreases. In Fig. 3, our results also suggest that when the daughter vesicle is large, the mother vesicle feels more uncomfortable. Consequently, the large daughter vesicle is then expelled with higher speed compared to the case of small daughter vesicle. However, the high speed will be decreased by the effect of barrier from the line tension energy.

IV. CONCLUSIONS

In this research, we study translocation phenomena of a vesicle through a narrow pore by using the Onsager principle. The first problem is the translocation of a vesicle through a hole in a solid membrane separating two chambers. We found that the translocation time decreases as the pressure difference across the membrane increases, or the initial size of the vesicle decreases as expected. The reaction paths obtained from the string method and the actual kinetic paths obtained from the Onsager principle are significantly different from each other if the external driving force is large. This suggests that the Onsager principle is an extension of the string method at large external driving force. For the second problem, we investigate the birthing process of a daughter vesicle in self-reproducing vesicle system. The equation of motion for the daughter vesicle is derived by using the Onsager principle. We found that the translocation time decreases when the friction caused by the hole against the motion of the daughter vesicle decreases. When the daughter vesicle is large, the mother vesicle feels more uncomfortable. Consequently, the large daughter vesicle is then expelled with higher speed compared to the case of small daughter vesicle.

[1] P. Khunpetch, X. Man, T. Kawakatsu, and M. Doi, J. Chem. Phys. **148**, 134901 (2018).

Acknowledgements

I am exceedingly grateful to my supervisor Prof. Toshihiro Kawakatsu. He always gives me inspirations and shows me how to be a good physicist. I really appreciate all his suggestions and answers to my questions. His physical intuitions make me amaze through his simple examples. Apart from doing research with him, I am really grateful to him for giving me the opportunity for coming to Japan and continuing my Ph.D. study.

I would also like to thank Prof. Masao Doi for introducing me the vesicle translocation problem when I was doing my internship at Beihang university, China. After returning to Japan, we still continued solving the problem until the final result appeared. He gave me lesson on taking action seriously. I greatly appreciate his suggestions and encouragements.

I would like to thank everyone in our group: especially, Hiroshi Yokota for helping me from the simplest things, for example, writing my name in Katakana or going to bank with me to the most complicated thing like filling out scholarship form. I would also like to thank Yoko Wako. I appreciate all the work she has done to help me.

My life in Sendai would be unenjoyable without Thai students whom I have met at Urban Castle Kawauchi (UCK). I would like to thank them for giving me fond Sendai memories. Eating Sukiyaki and talking on Friday night is the best way to relax after doing hard research for whole week. I hope to see all of you again in Thailand !

Spending time with international students at UCK is also unforgettable. I have learned various cultures, languages, and aspects from them. I hope, I can meet them again somewhere in the world.

Finally, I would like to thank my parents who always support, understand and believe in me.

Contents

Chapter **page**

CHAPTER I

Introduction

1.1 Motivation

Vesicles are considered as one of the main components of life. Vesicles consist of a bilayer membrane of amphiphilic molecules that are composed of a "water-loving (polar)" head-group and a "water-avoiding" hydrocarbon chains. Amphiphilic lipid molecules play a role in the evolution from molecular assembly to cellular life [1], [2], [3]. Soap and detergent are common amphiphilic substances that we can see in everyday life. Due to hydrophobic interactions of the hydrocarbon chains, the amphiphilic molecules start to assemble spontaneously into two layers held together by non-covalent forces when the concentration in aqueous solution is high enough [4], [5]. In order to avoid the interaction with water at the edge of the membrane, the bilayer forms a closed surface called a vesicle. Even though the membrane of vesicle has a thickness of typically a few nanometers, the size of vesicle can be in the order of up to 100 micrometers. Due to external conditions lipid bilayer vesicles show a wide variety of shape deformation. Their remarkably flexible surfaces attract researchers for many decades [6], [7]. Here, we will give some examples of shape transitions of fluid bilayer vesicles induced by changing area-to-volume ratio due to temperature variations.

Our first example of a vesicle shape deformation is budding transition. Figure 1.1 shows a series of images of L-α-dimyristoylphosphatidylcholine (DMPC) bilayer vesicle in a pure water prepared at different temperatures. The vesicle has a simple spherical shape at the lowest temperature but it becomes increasingly

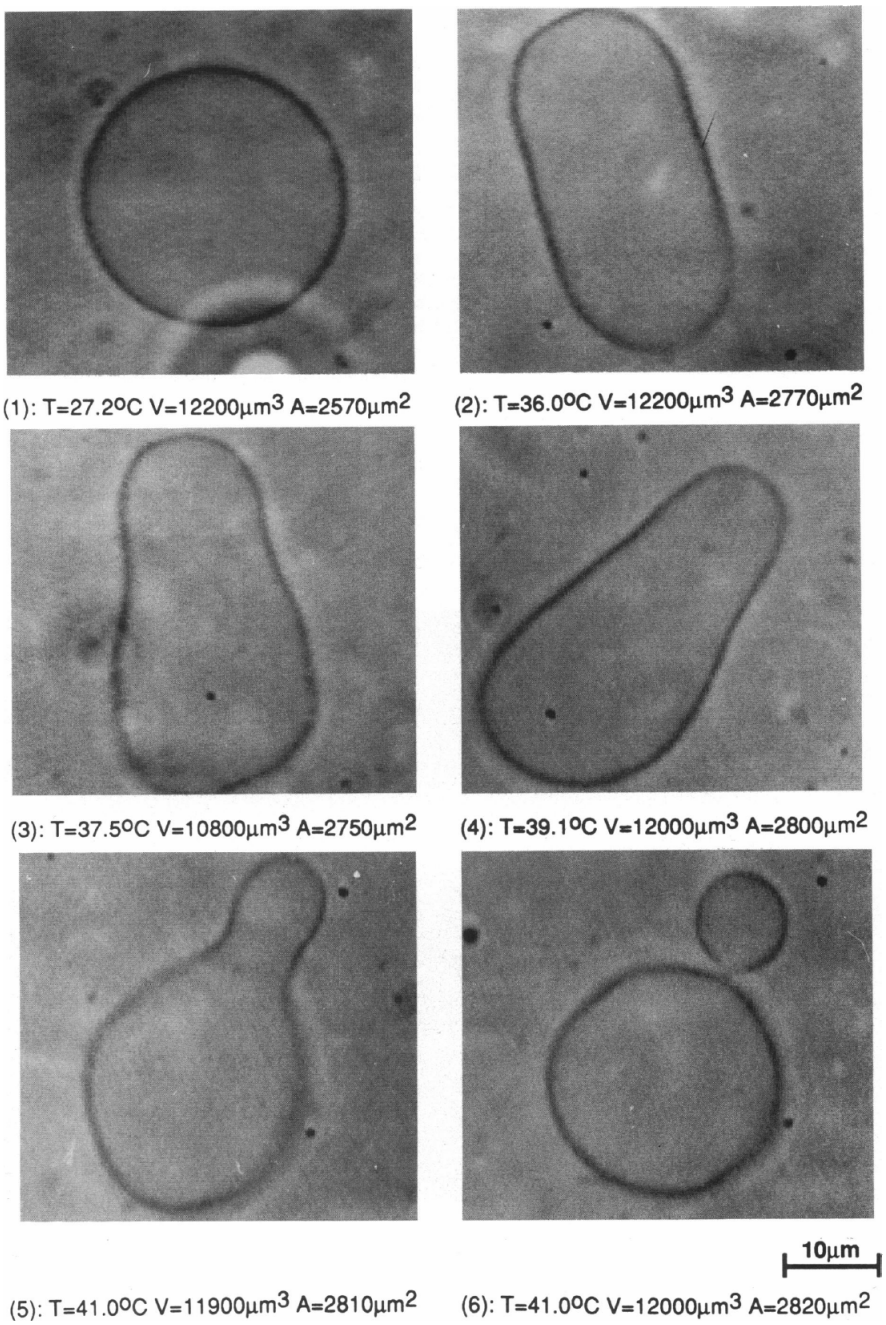

Figure 1.1: A typical budding transition of a vesicle [8]. The prolate ellipsoid and pear shapes are stable in the temperature between 27.2°C and 40.9°C. Further increasing the temperature by 0.1°C the pear shape becomes unstable and goes into the budded state at 41.0°C.

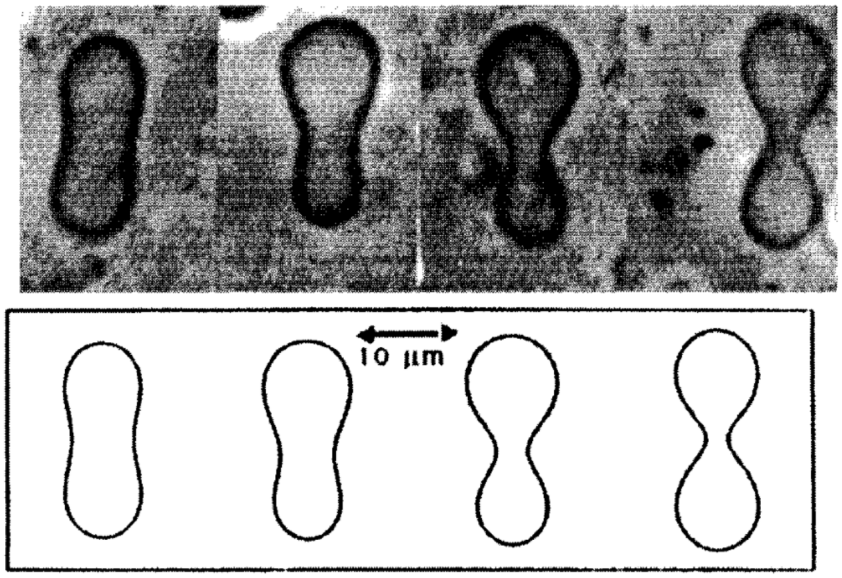

Figure 1.2: Re-entrant transition. From left to right, the temperature increases from 20.7, 32.6, 40.0, and 44.3°C, respectively. The lower figure shows the contour of stationary shapes [9].

rod-like (prolate ellipsoid) when the temperature is increased. During the increasing of the temperature, the vesicle surface area is increased, while the vesicle volume remains unchanged. As the temperature is increased further, the vesicle becomes more and more pear-shaped. In the temperature regime between 27.2°C and 40.9°C the ellipsoidal and pear shapes are stable. At 41.0°C the pear shape suddenly becomes unstable going into the budding shape. By further changing the area-to-volume ratio, the neck closes and the vesicle becomes two spherical vesicles connected by a narrow bilayer cylinder.

The budding transition described above does not always occur when the temperature is increased. Sometimes the up/down reflection symmetry is restored among further heating. The situations are shown in the re-entrant transition as shown in Fig. 1.2. Furthermore, spherical vesicle can become a pancake-shape (oblate ellipsoid) after increasing of the temperature. The vesicle then develops into a discocyte and, consequently, transforms into a stomatocyte as shown in Fig. 1.3. This transformation is very interesting because the discocyte shapes are

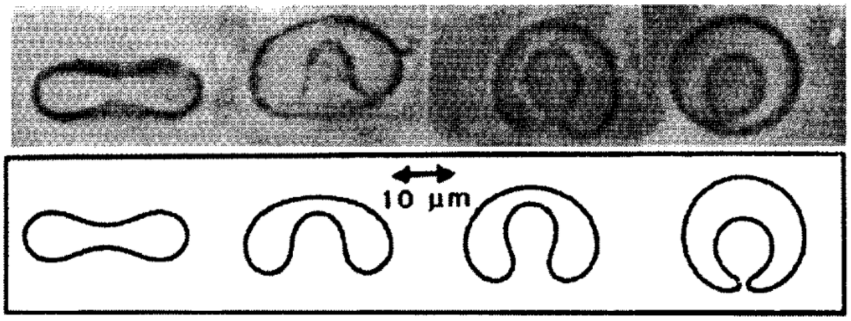

Figure 1.3: Discocyte-stomatocyte transition. From left to right, the temperature increases from 43.8, 43.9, 44.0, and 44.1°C, respectively. The theoretical curves are shown in the lower figure [9].

very similar to the shape of red blood cells when they are at rest. In fact, many attempts on the study of vesicles shape change are motivated from the questions for understanding the shape of red blood cells. Examples of these observations suggest two essential physical properties of the typical lipid bilayer vesicles. First, fluidity is the important property of bilayer membranes because, if the membranes resisted shear, these shape deformations are hardly observable. However, the bilayer structure is also robust because pores or holes are not formed, while the vesicle shape deforms significantly and topology of the bilayer vesicles does not change (In the budding transition, as we mentioned, the buds are not cut from the mother vesicles, but connected together by a bilayer cylinder.).

By using laser tweezers, the dynamics of lipid bilayer vesicles induced by changing external parameters becomes accessible. Considering bilayer membranes as two-dimensional surfaces embedded in three-dimensional space, the theoretical description on this mesoscopic length scales is introduced independently more than forty years ago in three seminal papers [10], [11], [12]. The bilayer configurations are fundamentally determined by bending elasticity. This fundamental property is the reason why there is a wide variety of non-spherical shapes of vesicles. Bending elasticity not only causes a large variety of vesicle shapes, but also leads to various dynamical properties. The dynamical aspect of vesicles, especially, the translocation through a small hole due to external driving forces is

an interesting problem. The mechanism is relevant to, for example, many transdermal applications [13], [14], transendothelial migration in immune system [15] and drug delivery in pharmacological research [16], [17], [18]. The translocation phenomena of a vesicle through a small hole are the subject matter of this thesis. Before going into details, we will give a brief review of previous studies on such a filtration process. The interesting question is that how the effectiveness of such filtration process depends on various parameters of the system such as the driving forces, bending and stretching moduli of the vesicle, the initial size of the vesicle, and geometry and size of the hole. Theoretical studies using Monte Carlo simulations done by Linke *et al.* [19] and Gompper *et al.* [20] gave us an example of how driving force affects the process. In Ref. [19], their simulation results indicate that the osmotic pressure alone is sufficient to overcome the barrier caused by thermal fluctuations of the membrane shape. The translocation time is calculated and it is found that the translocation time is of the order of minutes. Gompper *et al.* [20] showed clearly that the vesicle can move through the narrow, cylindrical pore when the linear driving field is larger than the threshold value. Moreover, the mobility of the vesicle saturates at a value which is independent of the strength of the driving field. The threshold value of the driving field increases when the pore size is decreased as well as membrane area and bending rigidity increase. This behavior is in agreement with the experiment reported in Ref. [21]. Recently, Shojaei *et al.* [22] reported results of a theoretical study of translocation of an incompressible vesicle through a narrow pore by adopting the same model as that of Deserno *et al.* [23]. In the work of Shojaei *et al.* [22], the energy for the vesicle shape is described by a bending modulus and a stretching modulus. Shojaei *et al.* [22] have considered the effect of various parameters on the translocation time by using the Fokker-Planck formalism. For each vesicle size, their results suggested that the translocation time decreases as the external driving force increases. At a given constant external driving force, their results showed that the effect of the stretching modulus on the translocation time is weaker than the bending modulus.

Deformation of a red blood cell when it translocates through a slit by an incoming flow is studied by Salehyar *et al*. [24]. They numerically investigate the dynamics by using a multiscale fluid-cell interaction model. Their results show that, depending on the initial orientation of the red blood cell, there are two different behaviours of the shape deformation during the translocation process. In the first behavior, the red blood cell forms a dumbbell shape when it is pushed through the slit. The second one is that the cell shows infolding where the membrane bends inwardly to form a concave region.

In our study, we focus on the kinetic pathway of the translocating vesicle. In order to study such a translocation process, we employ the string method to investigate the reaction path of the kinetic. The string method is a robust tool to obtain the reaction pathways [25], [26], [27]. The basic idea of the string method is to evolve paths (strings) according to the potential force in the normal directions to the path on the free energy landscape. The condition that at each point on the path the force perpendicular to the paths is zero gives the minimum energy paths (MEPs). On the other hand, the actual kinetic pathways of phase transitions can be obtained by using "Onsager variational principle" (or "Onsager principle" for short). The basic concept of the principle is the Onsager's reciprocal relation. This relation casts the slow dynamics of the system into variational principle, which bases on the existence of slow variables specifying slow dynamics of the system. The slow variables are characterized by that their relaxation time is distinctively larger than the other variables called fast variables. Our results show clearly that the reaction path obtained from the string method and the kinetic paths obtained from the Onsager principle are significantly different from each other when the pressure gradient is large. We also show that the translocation time of the vesicle decreases as the pressure difference increases, or the initial size of the vesicle decreases.

Another problem of such translocation process is the birthing of a vesicle through a pore in self-reproducing vesicle system. Previous studies done by various synthetic biology groups [30], [31], [32], [33], [34], [35], [36], [37] have

shown that binary vesicle constituting of two types of lipids with different molecular shape shows self-reproduction of a vesicle. However, the mechanism is still not been understood yet. Recently, Sakuma *et al.* [38] proposed a model self-reproducing vesicle system without adding molecules. In their model, the vesicle is composed of cylinder-shaped lipids [1, 2-dipalmitoyl-*sn*-glycero-3-phosphocholine (DPPC)] which has a high melting temperature $T_m = 41°C$ and inverse-cone-shaped lipids [1, 2-dilauroyl-*sn*-glycero-3-phosphoethano lamine (DLPE)] which has a low melting temperature $T_m = 29°C$. A phosphoethanolamine head group (PE lipids) is frequently noticed in topological transformations of the cellular membrane [39], [40], [41], [42]. This indicates that PE lipids have a role to induce topological transformations.

The birthing pathway observed by Sakuma *et al.* has shown in Fig. 1.4. The binary giant unilamellar vesicle (GUV) with a composition of DLPE/DPPC= 3/7 has a spherical shape at the temperature below the DPPC T_m (35°C) (Step 1). By increasing the temperature up to the temperature above the DPPC melting temperature $T_m = 42°C$, the GUV forms a stomatocyte shape due to an excess surface area compared with its inside volume in Step 2. The stomatocyte vesicle then forms an inclusion vesicle called the daughter vesicle inside it by plucking off the invagination neck (Step3). When the temperature is decreased below the melting temperature of the DPPC (35°C) the surface area of the mother vesicle decreases. This causes an increase in the membrane tension of the mother vesicle. To release this tension, the mother vesicle produces a pore and, then, the daughter vesicle is expelled through the pore, called the birthing of the daughter vesicle (Step 4). Due to the decrease in the line tension, the mother GUV recovers a spherical shape by closing the pore after the birthing. Although the recovered mother GUV is smaller than the original one, it follows the same pathway to produce the second daughter vesicle (green pathway in Fig. 1.4). Moreover, the daughter vesicle produces granddaughter vesicle via the same birthing pathway (red pathway in Fig. 1.4). Sometimes the birthing is maintained to fourth- or fifth-generation of vesicles.

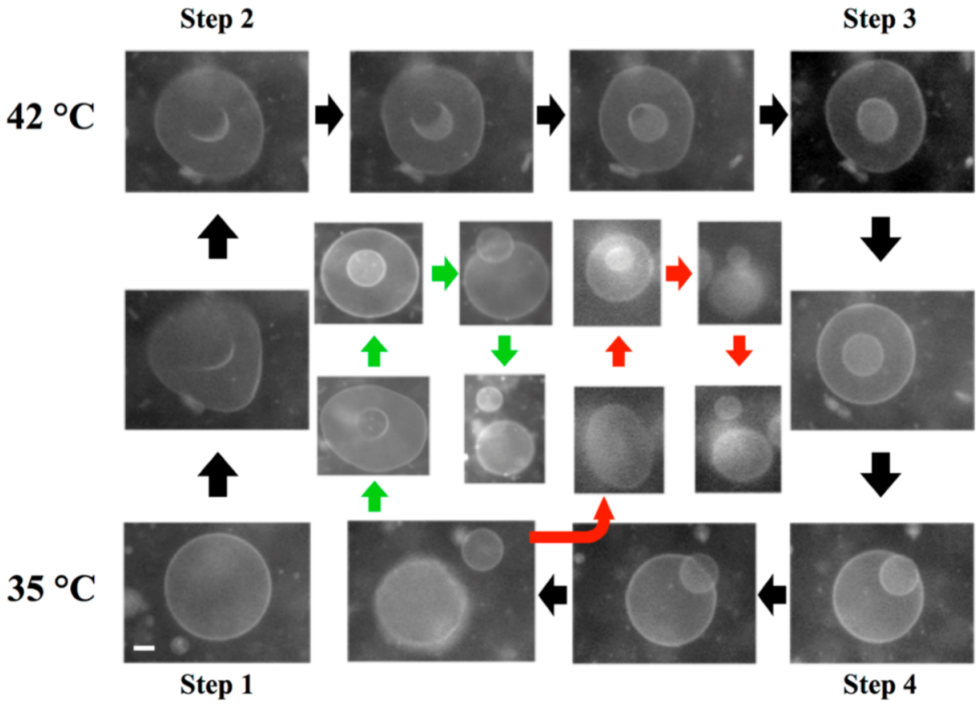

Figure 1.4: The observed birthing pathway of binary giant unilamellar vesicle constituting of [1, 2-dilauroyl-*sn*-glycero-3-phosphoethano lamine (DLPE)] and [1, 2-dipalmitoyl-*sn*-glycero-3-phosphocholine (DPPC)] with a composition of DLPE/ DPPC= 3/7. The birthing pathway composes of the following 4 steps. (Step 1) The spherical mother GUV forms a stomatocyte shape. (Step 2) The stomatocyte mother vesicle forms the daughter vesicle. (Step 3) The daughter vesicle is expelled through the pore, called the birthing of the daughter vesicle. (Step 4) The mother GUV recovered a spherical shape by closing the pore. The green pathway shows that the recovered mother vesicle follows the same pathway to produce the second daughter vesicle and the red pathway shows producing of the granddaughter vesicle by the daughter vesicle [1].

In our study, we theoretically model the birthing process of the daughter vesicle. We derive the free energy landscapes of the system and show clearly the disappearance of the energy barrier when the appropriate bending, stretching, and line tension moduli are selected. We, again, employ the Onsager principle to investigate kinetic of the system. Our results show the decreasing in the translocation when the friction decreases, or the size of the daughter vesicle decreases.

1.2 Outline of the Thesis

We begin the Chapter 2 by giving a brief review of the Onsager variational principle. In this thesis, we will explain the Onsager principle by taking a problem in hydrodynamics. We will show that the principle is an extension of Rayleigh's principle of the least energy dissipation which based on the existence of Rayleigh's dissipation function. The recipe of making kinetic equations from the Onsager principle will be given. To demonstrate how the principle works, we will apply the principle to study the problem of a droplet translocating through a hole across a membrane. We end this chapter by introducing the Helfrich free energy which is an important concept for studying the problem of a vesicle translocating through a pore.

In Chapter 3, the string method which is a tool for determining the kinetic pathway will be described. We give some examples of the application of the string method for calculating the minimum energy paths in the end of this chapter.

In Chapters 4 and 5 we will examine the translocation process of a vesicle through a small pore. In Chapter 4, we will study translocation process of a vesicle through a hole in a solid membrane separating two chambers. By considering the stretching energy of the vesicle and the driving force due to pressure difference, we derive a free energy that shows clearly the decreasing in the energy barrier as the pressure difference between two sides of the membrane increases. The difference between the reaction path obtained from the string method and the actual kinetic paths obtained from the Onsager principle is discussed when the friction parameter

changes. The translocation time decreases as the pressure difference increases, or the initial size of the vesicle decreases.

Chapter 5 is devoted to the birthing process of a daughter vesicle in self-reproducing vesicle system. We will present a simple theoretical model on the birthing process of a single, rigid daughter vesicle through a pore. We derive a free energy that includes the bending, stretching and line tension energies. Our results show clearly the disappearance of the energy barrier with different values of bending, stretching, and line tension moduli. The effect of adding more water into the mother vesicle will also be discussed. The kinetic of the system will be studied by employing the Onsager principle. Our results indicate that translocation time decreases as the friction parameter decreases, or the initial size of the daughter vesicle decreases. We close this chapter with conclusions of the study.

Finally, we end this thesis with Chapter 6. This chapter will give a brief summary and conclusion of all results obtained under the investigation pursued in this study.

CHAPTER II

Methodology and the Simplest Example

In this chapter, we will give a brief review of the physical theories used in the present thesis. We shall first discuss the Onsager variational principle (or "Onsager principle" for short) which is useful for deriving the equations of motion for the translocating vesicle. Onsager principle is originally proposed by L. Onsager [43], [44]. The basic concept of the principle is the Onsager's reciprocal relation. The relation casts the slow dynamics of the system into a variational principle which bases on the existence of slow variables specifying slow dynamics of the system. The principle has been shown to be useful for deriving time evolution equations in many soft matter systems such as diffusion equations for particles in dilute and in concentrated solutions [45] [46], kinetic equations in gel dynamics [46] [47], Cahn-Hilliard equations in phase separation [48] etc.

We first discuss sedimentation of a particle in a viscous fluid in Subsec. 2.1.1. The friction coefficient for the case of rigid sphere is evaluated in Subsec. 2.1.2. We discuss the variational principle for motion of particles in viscous fluids in Subsec. 2.1.3. Subsection 2.1.4 describes the Onsager principle in a more general form of the variational principle. We give a summary of the derivation of the kinetic equations by using the principle in Subsec 2.1.5. In Sec 2.2, we will give the simplest example of using Onsager principle: translocation of a droplet through a narrow hole across a membrane. We end this chapter by introducing the Helfrich free energy for membrane which is an important concept for studying translocation

of a vesicle through a pore.

2.1 Onsager Variational Principle

The Onsager principle is an extension of Rayleigh's principle of the least dissipation of energy. Here, we will consider the problem in hydrodynamics, i.e., the dynamics of particle-fluid systems. Small particles moving in a viscous fluid, e.g., particles sedimenting in a fluid, can be described by the force balance between the potential force and the frictional force. The reciprocal relation for the friction coefficient allows us to write such the balance of two forces in the form of a variational principle. Onsager noticed that many phenomenological equations describing the time evolution of the non-equilibrium systems can be written in a form of particle-fluid system. He then proved that the reciprocal relation must hold for such a kind of time evolution equation. This casts the evolution law of such systems into a variational principle called the Onsager variational principle which bases on the existence of slow variables. The slow variables are characterized by their relaxation time, which are distinctively larger than the other variables called fast variables.

2.1.1 Sedimentation of a Particle in a Viscous Fluid

We consider sedimentation of a particle of mass m in a viscous fluid under gravitational force (see Fig. 2.1). Let $\mathbf{x} = (x_1, x_2, ..., x_f)$ be generalized coordinates specifying the state of the particle, where f is the degree of freedom of the system. For a rigid particle, f is 6 and x_i are the position and orientation of the particle. Let $U(\mathbf{x})$ be the gravitational potential energy. The gravitational force is

$$\mathbf{F} = m\mathbf{g} = -\frac{\partial U(\mathbf{x})}{\partial \mathbf{x}}. \tag{2.1}$$

In the limit of small Reynolds number, the frictional force is proportional to the velocity of the particle:

$$\mathbf{F_f} = -\zeta \dot{\mathbf{x}}, \tag{2.2}$$

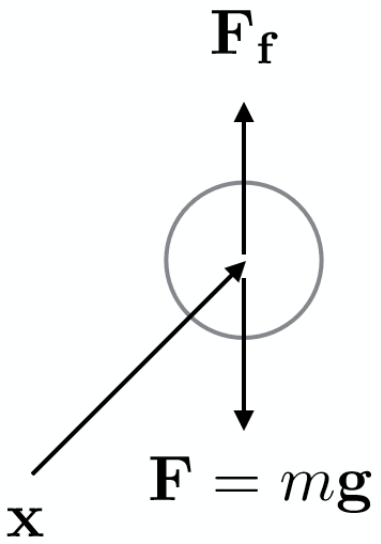

Figure 2.1: The balance between two forces acting on a particle with mass m sedimenting in a viscous fluid.

where ζ is the friction coefficient.

Since the Reynolds number is assumed to be negligibly small in Stokesian hydrodynamics, the gravitational force must be balanced with the frictional force as

$$\zeta \dot{\mathbf{x}} = -\frac{\partial U(\mathbf{x})}{\partial \mathbf{x}}. \tag{2.3}$$

2.1.2 Friction Constant for a Rigid Sphere

We proceed to discuss the friction constant for the case of a rigid sphere [57]. In the absence of external force, we consider a sphere of radius r moving with instantaneous velocity $\mathbf{v}_0$ in an infinite, viscous, incompressible fluid. The situation is shown in Fig. 2.2. In such a situation, the Navier-Stokes equation reduces to

$$0 = -\nabla\Big(P - \frac{\eta}{3}\nabla \cdot \mathbf{v}\Big) + \eta\nabla^2\mathbf{v}, \tag{2.4}$$

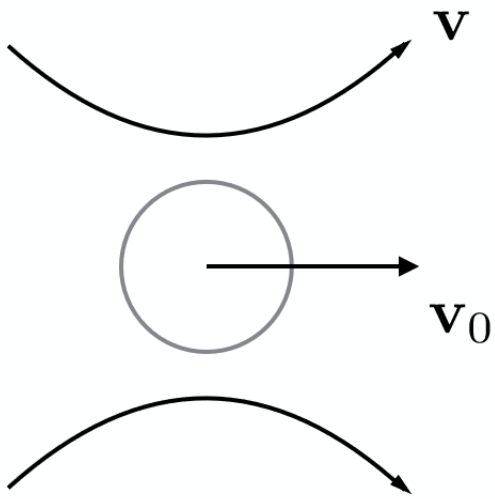

Figure 2.2: The rigid sphere moving in the viscous fluid. The sphere has instantaneous velocity $\mathbf{v}_0$, while the fluid velocity is denoted as $\mathbf{v}$.

where the fluid has a viscosity η and $\mathbf{v(x)}$ is the velocity field of the fluid. We assume that the material derivative of $\mathbf{v}$ is small compared to the viscous terms. Since there is no source for the fluid, the incompressibility condition $\nabla \cdot \mathbf{v} = 0$ must satisfy everywhere. Then, the dynamics of the particle can be described by the coupled equations

$$\nabla^2 \mathbf{v} = \frac{1}{\eta} \nabla P, \tag{2.5}$$

and

$$\nabla \cdot \mathbf{v} = 0, \tag{2.6}$$

where the fluid sticking to the sphere boundary condition is given. We choose the center of the sphere to be the origin of the coordinate system. Any points in space are specified by the cartesian coordinates (x, y, z) or the spherical coordintes (r, θ, ϕ). The sphere is at rest at the origin and the fluid flows with uniform constant velocity $\mathbf{v_0}$ at infinity. The boundary conditions become

$$\mathbf{v}(\mathbf{r})|_{r=a} = 0, \tag{2.7}$$

and

$$\mathbf{v}(\mathbf{r}) \xrightarrow[r\to\infty]{} \mathbf{v_0}, \tag{2.8}$$

while the Eqs. (2.5) and (2.6) remain invariant under the translation.

By taking the divergence of Eq. (2.5) and using Eq. (2.6), we obtain the Laplace's equation

$$\nabla^2 P = 0. \tag{2.9}$$

In spherical polar coordinates, the solution must be a linear superposition of solid harmonics. We can write the solution as

$$P = P_0 + \eta P_1 \frac{\cos\theta}{r^2}, \tag{2.10}$$

and, to determine the coefficients P_0 and P_1, Eqs. (2.5) and (2.6) must be satisfied. Then, the problem now is to solve the inhomogeneous Laplace's equation, which is derived from Eqs. (2.5) and (2.10)

$$\nabla^2 \mathbf{v} = P_1 \nabla \frac{\cos\theta}{r^2}, \tag{2.11}$$

with the conditions

$$\mathbf{v}(\mathbf{r})|_{r=a} = 0, \tag{2.12}$$

and

$$\mathbf{v}(\mathbf{r}) \xrightarrow[r\to\infty]{} \mathbf{v}_0. \tag{2.13}$$

Equation (2.11) gives a particular solution

$$\begin{aligned} \mathbf{v}_1 &= -\frac{P_1}{6} r^2 \nabla \frac{\cos\theta}{r^2} \\ &= -\frac{P_1}{6}\Big(\frac{\hat{\mathbf{z}}}{r} - 3\mathbf{r}\frac{z}{r^3}\Big), \end{aligned} \tag{2.14}$$

where $\hat{\mathbf{z}}$ denotes the unit vector in the z direction. We can easily verify that Eq. (2.14) is the solution of Eq. (2.11), as follows:

$$\begin{aligned} \nabla^2 \mathbf{v}_1 &= -\frac{P_1}{6}\Big[-3\nabla^2\Big(\frac{\mathbf{r}z}{r^3}\Big)\Big] \\ &= P_1 \nabla\Big(\frac{z}{r^3}\Big) \\ &= P_1 \nabla \frac{\cos\theta}{r^2}. \end{aligned} \tag{2.15}$$

To obtain the complete solution, we add the appropriate homogeneous solution to Eq. (2.14) which satisfies the conditions Eqs. (2.12) and (2.13). The complete solution is

$$\mathbf{v} = \mathbf{v}_0\Big(1 - \frac{a}{r}\Big) + \frac{1}{4} v_0 a (r^2 - a^2) \nabla \frac{\cos\theta}{r^2}, \tag{2.16}$$

where

$$P_1 = -\frac{3}{2} v_0 a, \tag{2.17}$$

for satisfying Eq. (2.6).

The force per unit area acting on the sphere by the fluid is given by

$$\mathbf{f} = -\hat{\mathbf{r}} \cdot \overleftrightarrow{P}, \tag{2.18}$$

where $\hat{\mathbf{r}}$ is the unit vector in the radial direction and the tensor $\overleftrightarrow{P}$ is given by

$$P_{ij} = \delta_{ij} P - \eta\left[\left(\frac{\partial v_i}{\partial x_j} + \frac{\partial v_j}{\partial x_i}\right) - \frac{2}{3}\delta_{ij} \nabla \cdot \mathbf{v}\right]. \tag{2.19}$$

The $i-$th component of the vector $\hat{\mathbf{r}} \cdot \overleftrightarrow{P}$ is

$$\begin{aligned}\left(\hat{\mathbf{r}} \cdot \overleftrightarrow{P}\right)_i &= \frac{1}{r} x_j P_{ji} \\ &= \frac{1}{r} x_j \left[\delta_{ji} P - \eta \left(\frac{\partial v_j}{\partial x_i} + \frac{\partial v_i}{\partial x_j} \right) \right] \\ &= \frac{x_i}{r} P - \frac{\eta}{r} \left[\frac{\partial}{\partial x_i}(x_j v_j) - v_i + x_j \frac{\partial}{\partial x_j} v_i \right]. \end{aligned} \tag{2.20}$$

Then, $\mathbf{f}$ becomes

$$\mathbf{f} = -P\hat{\mathbf{r}} + \frac{\eta}{r}[\nabla(\mathbf{r} \cdot \mathbf{v}) - \mathbf{v} + (\mathbf{r} \cdot \nabla)\mathbf{v}], \tag{2.21}$$

where $P = P_0 + \eta P_1(\cos\theta / r^2)$, $P_1 = -(3/2)v_0 a$, and $\mathbf{v}$ is given by Eq. (2.16). Because $\mathbf{v}(\mathbf{r})|_{r=a} = 0$, the second term in the bracket vanishes. We need to verify the first term and the last terms in the bracket at $r = a$. We can show that the first term becomes zero and the last term is

$$\frac{1}{r}[(\mathbf{r} \cdot \nabla)\mathbf{v}]_{r=a} = \frac{3}{2}\left(\frac{\mathbf{v}_0}{a}\right) - \frac{3}{2} v_0 \left(\frac{\cos\theta}{a}\right)\hat{\mathbf{r}}. \tag{2.22}$$

By substituting Eq. (2.22) into Eq. (2.21), we obtain

$$\mathbf{f}_{r=a} = -P_0 \hat{\mathbf{r}} + \frac{3}{2}\frac{\eta}{a}\mathbf{v}_0. \tag{2.23}$$

The total force acting on the sphere by the fluid is

$$\mathbf{F}_\mathbf{f} = \oint dA\, \mathbf{f}, \tag{2.24}$$

where dA is a surface element of the sphere. Using Eq. (2.23), we obtain Stokes' law

$$\mathbf{F}_\mathbf{f} = 6\pi\eta a \mathbf{v}_0. \tag{2.25}$$

The first term in Eq. (2.23) does not contribute to force on the sphere due to symmetry. Owing to the definition of the friction constant

$$\mathbf{F}_\mathbf{f} = -\zeta \mathbf{v}_0, \tag{2.26}$$

we obtain the friction coefficient for the sphere as

$$\zeta = 6\pi\eta a. \tag{2.27}$$

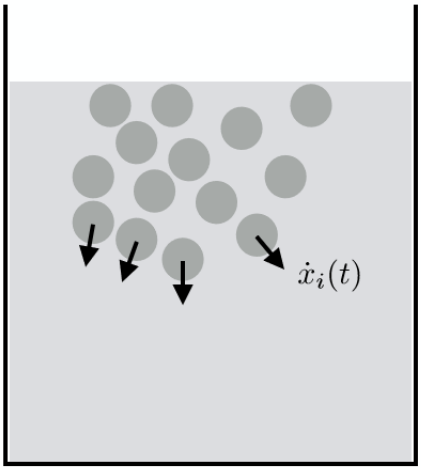

Figure 2.3: A collection of particles sedimenting in a viscous fluid.

2.1.3 Variational Principle for Motion of Particles in Viscous Fluids

Here we will discuss the variational principle for particle-fluid systems. Let us consider many particles moving in a viscous fluid. An example of this system is particles sedimenting under a gravity (see Fig. 2.3).

The system is described by a set of generalized coordinates $\mathbf{x} = (x_1, x_2, ..., x_f)$ specifying the sate of the system. Let $U(\mathbf{x})$ be the potential energy of the system. The potential energy can be a gravitational potential energy or the interaction energy between the particles. The potential force conjugate to the coordinate x_i is then written as

$$F_i = -\frac{\partial U(\mathbf{x})}{\partial x_i}. \tag{2.28}$$

When the particles move in a viscous fluid, the fluid exerts a frictional force

against the motion of the particles. In the limit of small Reynolds number, the frictional force is a linear function of the generalized velocity $\dot{x}_j$ [49] which is given by

$$F_{fi} = -\sum_j \zeta_{ij}\dot{x}_j, \tag{2.29}$$

where ζ_{ij} are the friction coefficients. Usually, ζ_{ij}'s are functions of $\mathbf{x}$ and they satisfy the following two properties:

(i) the Lorentz reciprocal relation

$$\zeta_{ij} = \zeta_{ji}, \tag{2.30}$$

and

(ii) the positive definiteness

$$\sum_{i,j} \zeta_{ij}\dot{x}_i\dot{x}_j \geq 0 \quad \text{for any } \dot{x}_i. \tag{2.31}$$

By using the reciprocal relation, we can write the frictional force as

$$F_{fi} = -\frac{\partial \Phi}{\partial \dot{x}_i}, \tag{2.32}$$

where Φ is called the Rayleigh's dissipation function defined by

$$\Phi = \frac{1}{2}\sum_{i,j} \zeta_{ij}\dot{x}_i\dot{x}_j.^{1} \tag{2.33}$$

Since we have assumed that the Reynolds number is negligibly small, the time evolution of the particles can be described by the frictional force and the potential force where these two forces need to be balanced, i.e.,

$$\sum_j \zeta_{ij}\dot{x}_j = -\frac{\partial U(\mathbf{x})}{\partial x_i}, \tag{2.34}$$

where we have neglected the random forces regarding as the particles are sufficiently large. The inertia forces are also assumed to be negligibly small. Then, the time evolution equation for x_i can be written as

$$\frac{dx_i}{dt} = -\sum_j (\zeta^{-1})_{ij}\frac{\partial U(\mathbf{x})}{\partial x_j}, \tag{2.35}$$

[1]Notice that since $\partial\Phi/\partial\dot{x}_i$ gives $(1/2)\Sigma_j(\zeta_{ij} + \zeta_{ji})\dot{x}_j$, to get the frictional force Eq. (2.29), the reciprocal relation is really needed.

where $(\zeta^{-1})_{ij}$ is the ij-component of the inverse of the matrix ζ_{ij}.

Next, let us consider the following quadratic function of $\dot{\mathbf{x}} = (\dot{x_1}, \dot{x_2}, ..., \dot{x_f})$,

$$R(\dot{\mathbf{x}}) = \frac{1}{2}\sum_{i,j}\zeta_{ij}\dot{x}_i\dot{x}_j + \sum_i \frac{\partial U(\mathbf{x})}{\partial x_i}\dot{x}_i. \tag{2.36}$$

Since $\sum_{i,j}\zeta_{ij}\dot{x}_i\dot{x}_j \geq 0$, $R(\dot{\mathbf{x}})$ has a unique minimum as a function of $\dot{\mathbf{x}} = (\dot{x_1}, \dot{x_2}, ..., \dot{x_f})$ when the conditions $\partial R/\partial \dot{x}_i = 0$ are satisfied. We can see that this condition gives us the time evolution for x_i in the same manner as the force balance equation Eq. (2.34). This is the variational principle for motion of particles in viscous fluids. This principle is called the principle of least energy dissipation, first introduced by Rayleigh [59]. The function $R(\dot{\mathbf{x}})$ is called the Rayleighian of the system. It is sum of dissipation function and time derivative of the potential energy, i.e.,

$$R = \Phi + \dot{U}, \tag{2.37}$$

where Φ is given by Eq. (2.33) and $\dot{U}$ is defined by

$$\sum_i \frac{\partial U(\mathbf{x})}{\partial x_i}\dot{x}_i. \tag{2.38}$$

It should be noted that the principle of least energy dissipation is based on the existence of Rayleigh's dissipation function. The minimization of Rayleighian is performed over the rate of change of the coordinate of the system, $\dot{x}$, rather than on the coordinate x. It is the competition between dissipation and rate of change of the energy. One can give a physical interpretation of the dissipation function. Let us consider the work done by the system against friction given by

$$\begin{aligned} dW_f &= -\mathbf{F_f}\cdot d\mathbf{x} \\ &= -\mathbf{F_f}\cdot \mathbf{v}dt \end{aligned} \tag{2.39}$$

In the limit of small Reynolds number, dW_f gives

$$(\zeta_x v_x^2 + \zeta_y v_y^2 + \zeta_z v_z^2)dt = 2\Phi dt. \tag{2.40}$$

Hence, 2Φ is the rate of energy dissipation due to friction.

2.1.4 Onsager Variational Principle

In the previous section, we have shown that the variational principle gives us the time evolution equation for particle-fluid systems in the same form as force balance, where the configuration of the particles is described by a set of generalized coordinates $\mathbf{x} = (x_1, x_2, ..., x_f)$. Here let us consider non-equilibrium system where the state of the system is described by the state variables $\mathbf{x} = (x_1, x_2, ..., x_f)$ and assume that the kinetic equation is of the following form

$$\frac{dx_i}{dt} = -\sum_j \mu_{ij}(\mathbf{x}) \frac{\partial A(\mathbf{x})}{\partial x_j}, \tag{2.41}$$

where $A(\mathbf{x})$ is the free energy of the system and the coefficients $\mu_{ij}(\mathbf{x})$ are called the kinetic coefficients corresponding to the inverse of the friction coefficients $(\zeta^{-1})_{ij}$ in Eq. (2.35). We can see that Eq. (2.41) and Eq. (2.35) have the same form. As long as the time evolution of the system is described by Eq. (2.41) the kinetic coefficients μ_{ij} must satisfy the reciprocal relation

$$\mu_{ij} = \mu_{ji}. \tag{2.42}$$

Therefore the kinetic equations as shown in Eq. (2.41) can be translated into the variational principle. We then can write the Rayleighian of the system as

$$R(\dot{\mathbf{x}}) = \frac{1}{2} \sum_{i,j} \zeta_{ij} \dot{x}_i \dot{x}_j + \sum_i \frac{\partial A(\mathbf{x})}{\partial x_i} \dot{x}_i, \tag{2.43}$$

which is sum of the dissipation function and time derivative of the free energy

$$R = \Phi + \dot{A}. \tag{2.44}$$

By minimizing the Rayleighian R with respect to $\dot{x}_i$, we can obtain the time evolution of the system. This is the Onsager variational principle or simply Onsager principle [43], [44], [45]. The important point in the Onsager principle is that the state variables $\mathbf{x} = (x_1, x_2, ..., x_f)$ change much more slowly than the other variables. We shall call this set of state variables "slow variables". The slow variables are characterized by using their relaxation time, which are distinctively larger than the other variables called "fast variables".

As we said, Onsager principle is an extension of Rayleigh's principle of the least dissipation of energy because he showed that the principle holds for general irreversible processes. The essential physical assumption for the irreversible process is that the fluxes depend linearly on the thermodynamic forces that causes them, e.g., Ohm's law for electrical conduction and Fick's law for diffusion. In the original paper published in 1953 [60], Onsager and Machlup formulated the variational principle as the extremum of the function $\dot{S} - \Phi$, where $\dot{S}$ is the rate of production of entropy. This variational principle is formally equivalent to the physical assumption described above.

2.1.5 Recipe to Make Kinetic Equations

Here we will give a summary of making kinetic equations for non-equilibrium systems by using the Onsager principle.

(1) Choose proper slow variables $\mathbf{x} = (x_1, x_2, ..., x_f)$

In order to apply the principle to the practical problems, we first need to choose slow variables specifying slow dynamics of the system. How do we choose slow variables ? Because the slow variables specify the non-equilibrium state of the system, they must satisfy the following two conditions

(i) The set of the slow variables $\mathbf{x} = (x_1, x_2, ..., x_f)$ must be a complete set to describe the slow dynamics of the system. If the slow variables $\mathbf{x} = (x_1, x_2, ..., x_f)$ at time t is given, we should uniquely determine the set of the slow variables at time $t + \Delta t$.

(ii) The relaxation time of the slow variables are distinctively longer than the other variables.

(2) Construct the dissipation function of the system $\Phi(\mathbf{x}) = (1/2)\Sigma_{i,j}\zeta_{ij}\dot{x}_i\dot{x}_j$

(3) Construct the free energy of the system $A(\mathbf{x})$

(4) By minimizing the Rayleighian

$$\begin{aligned} R &= \Phi + \dot{A} \\ &= \frac{1}{2}\sum_{i,j}\zeta_{ij}\dot{x}_i\dot{x}_j + \sum_i \frac{\partial A}{\partial x_i}\dot{x}_i \end{aligned} \tag{2.45}$$

with respect to $\dot{x}_i$, i.e., $\partial R/\partial \dot{x}_i = 0$, it gives the equation of motion

$$-\sum_j \zeta_{ij}\dot{x}_j - \frac{\partial A}{\partial x_i} = 0. \tag{2.46}$$

2.2 The Simplest Example: Translocation of a Droplet Through a Narrow Hole Across a Membrane

Here we give the simplest example of using the Onsager principle: translocation of a droplet through a hole across a membrane. Structures and dynamics of a droplet suspended in a liquid attract researchers for decades [6]. Due to pressure difference between two sides of a membrane, a droplet can translocate through a small hole across the membrane. Effective filtration process depends on various parameters of the system such as pressure difference, an initial size of a droplet and pore sizes on a membrane, which is an interesting topic of study. In the petroleum industry, such a kind of process is used as one of the treatment techniques of oily wastewater [61].

Recently, there are progresses on the study of a droplet translocation. Darvishzadeh *et al.* [62] reported, in the absence of crossflow velocity, the dependence of critical pressure required for pushing an oil droplet across porous membranes in oil-in-water emulsions on a cylindrical pore with the pore radius size of micron by solving the Navier-Stokes equation numerically. Their results are consistent with the analytical prediction using the Young-Laplace pressure [63], [64].

In this example, we will use Onsager variational principle to study filtration process of a droplet. Our result in the dependence of the critical pressure on the

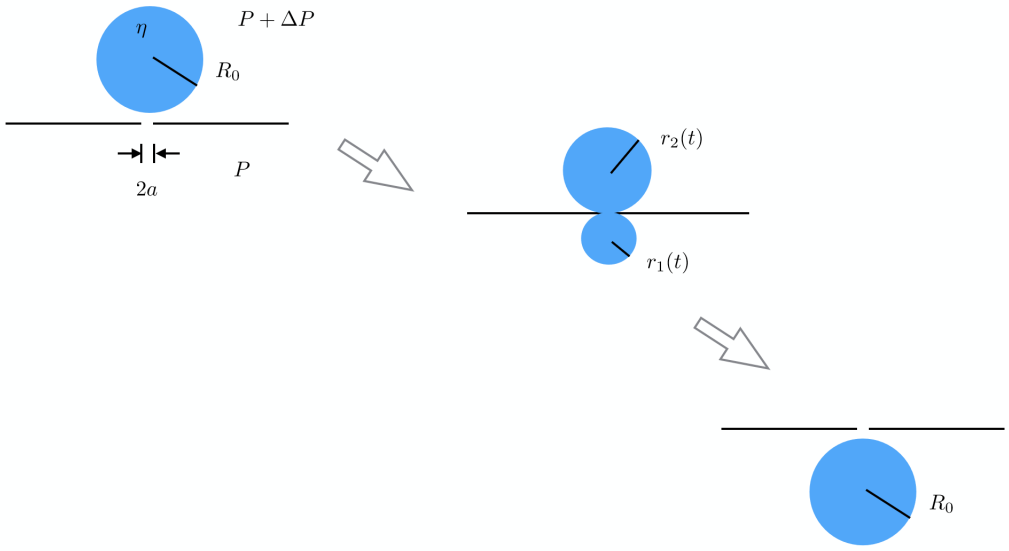

Figure 2.4: Model of a translocating droplet.

initial droplet size is in agreement with the result in [62]. We also consider the dependence of the translocation time on the pressure difference between both sides of a membrane, and on the initial size of a translocating droplet.

A. Theory of A Droplet

The shape of a translocating droplet is modeled by two connected spheres as illustrated schematically in Fig. 2.4. The translocating droplet has radii $r_1(t)$ and $r_2(t)$, where $r_1(t)$ and $r_2(t)$ stand for the radii of the above and below droplet, respectively. The initial size of the droplet is denoted by R_0 which is assumed to be much larger than the size of the narrow hole on the membrane and the thickness of the membrane is very small. Then we can neglect the structure of the hole and we consider the hole as a circle with radius a. The pressure is assumed to be constant at every point inside the droplet. The pressure difference between inside and outside of the spherical droplet is determined by the Laplace pressure. The liquid inside the droplet is assumed to be incompressible with viscosity η. Most of the energy dissipation is assumed to take place at the hole when the liquid is flowing through. The flow velocity is also assumed to be very small.

We use Onsager principle as an approximation scheme to derive a set of evolution equations for the droplet. The basic concept of the Onsager principle is the Onsager's reciprocal relation. This relation casts the slow dynamics of the system into variational principle. The remarkable relation in the principle, i.e. the reciprocal relation, bases on the existence of slow variables which specify slow dynamics of a system and their characteristic relaxation time is distinctively larger than the other variables, called fast variables.

If we have a set of slow variables $\mathbf{x} = (x_1, x_2, ..., x_f)$, Onsager principle is described by the minimization of Rayleighian defined by

$$R = \Phi + \dot{A}, \tag{2.47}$$

with respect to $\dot{x_i}$. Φ is the energy dissipation function and $\dot{A}$ is the time derivative of the free energy.

When the droplet is translocating through the hole, the slow variables describing its size are $r_1(t)$ and $r_2(t)$. However, we can further reduce the degrees of freedom to one using the constraint $R_0^3 = r_1^3 + r_2^3$. Because the translocation time of the droplet should depend on the initial size R_0 as well as the pressure difference ΔP across the membrane, we introduce dimensionless parameters, a/R_0 and $\Delta P a/\gamma$, where γ is the interfacial tension between the droplet and the liquid.

a. The potential energy

Because the translocating droplet's shape is assumed to be two connected spheres, the free energy is the sum of the surface tension energy and the work done by the pressure difference of each sphere:

$$A_{\rm dr} = \gamma 4\pi(r_1^2 + r_2^2) - \Delta P \frac{4\pi}{3}(r_1^3 - r_2^3). \tag{2.48}$$

Using the dimensionless variable and parameters we have introduced, the free energy is rewritten as

$$\begin{aligned} A_{\rm dr}\Big(x; \frac{a}{R_0}; \frac{\Delta P a}{\gamma}\Big) &= a^2\gamma\Big[4\pi\Big(\frac{R_0}{a}\Big)^2(x^{2/3} + (1-x)^{2/3}) \\ &\quad -\frac{4\pi}{3}\Big(\frac{R_0}{a}\Big)^3\Big(\frac{\Delta P a}{\gamma}\Big)(2x-1)\Big]. \end{aligned}$$

b. The energy dissipation function

In the limit of small Reynolds number, the energy dissipation function for the droplet takes the form

$$\Phi_{\rm dr} = \frac{1}{2}\zeta v_{\rm l}^2, \tag{2.50}$$

where the liquid flow velocity $v_{\rm l}$ is defined by $v_{\rm l} = (2r_1/a)^2\dot{r}_1$. We should mention that our flow velocity $v_{\rm l}$ is assumed to be proportional to ΔP. This dependence is different from the Orifice plate flowmeter which gives $v_{\rm l} \propto \sqrt{\Delta P}$ [65].

Next, we introduce the dimensionless variable x defined by $x = (r_1/R_0)^3$. Then, the energy dissipation function becomes

$$\Phi_{\rm dr}\Big(\dot{x}; \frac{a}{R_0}\Big) = \frac{8}{9}a^2\zeta\Big(\frac{R_0}{a}\Big)^6\dot{x}^2. \tag{2.51}$$

c. The droplet's evolution equation

To derive the evolution equation for the droplet, we minimize the Rayleighian, $R_{\rm dr} = \Phi_{\rm dr} + \dot{A}_{\rm dr}$ with respect to $\dot{x}$. This yields

$$\begin{aligned}\frac{dx}{d\tau'_{\rm dr}} &= -\frac{3\pi}{4}\Big(\frac{a}{R_0}\Big)^4\Big[(x^{-1/3} - (1-x)^{-1/3}) \\ &\quad -\Big(\frac{R_0}{a}\Big)\Big(\frac{\Delta P a}{\gamma}\Big)\Big],\end{aligned} \tag{2.52}$$

where $\tau'_{\rm dr} = t/\tau_{\rm dr}$ is a droplet-dimensionless time and $\tau_{\rm dr}$ is defined by $\tau_{\rm dr} = \eta a/\gamma$. We have assumed that, at the initial state, the bottom part of the droplet is a hemisphere with radius a and its center is located on the membrane. This gives $x(\tau'_{\rm dr} = 0) = (a/R_0)^3$.

B. Results and Discussions

We will show the results from our translocating droplet model. The experimental result done by F. Peters and D. Arabali [66] will be used to estimate the critical pressure and the translocation time for the droplet.

For completed translocation process, the pressure required for pushing the droplet can be obtained by solving Eq. 2.52 numerically. Figure. 2.5 shows clearly that, at $R_0/a = 10.0$, the critical pressure ΔP_c is $0.9\,\gamma/a$. By using the measured

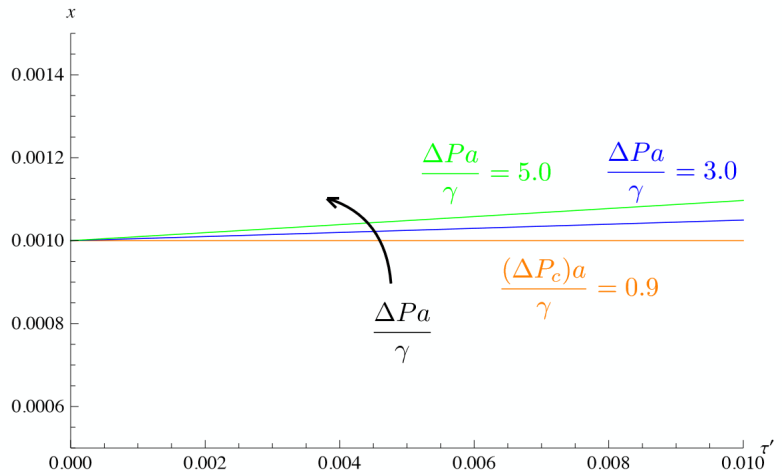

Figure 2.5: The evolution of the droplet. At $R_0/a = 10.0$, our representative result at short time scale shows the critical pressure $\Delta P_c = 0.9\,\gamma/a$. The horizontal axis is defined by $\tau'_{\rm dr} = \gamma t/\eta a$, where γ is the interfacial tension between the droplet and the liquid. η is the viscosity of the fluid inside the droplet. The vertical axis is defined by $x = (r_1/R_0)^3$.

interfacial tension γ between wacker silicone fluid AK20 (a poly dimethyl siloxane (PDMS)) with an kinematic viscosity of 20 $\mu\mathrm{m}^2\cdot\mathrm{s}^{-1}$ and water in the temperature range 18-35°C in [66] as an example, the critical pressure for the droplet will be estimated. At $T = 25$°C, the interfacial tension is of 35.87 $\mathrm{mN}\cdot\mathrm{m}^{-1}$. If the hole size a is of the order of micron, for $R_0/a = 10.0$, the critical pressure is $\Delta P_c \simeq 32.3$ kPa with the time scale $\tau_{\mathrm{dr}} = 0.54\,\mu$s, where the density of PDMS is of 965 $\mathrm{kg}\cdot\mathrm{m}^{-3}$. In Ref. [66], the oil drop contour data based on digital image processing are used to determine the interfacial tension. The authors proposed an explicit expression for the interfacial tension in terms of the measured quantities by using a force balance without involving the Laplace equation relating the pressure and curvature of the oil drop. Among a few data of the interfacial tension for the oil/water system, the authors' result in Ref. [66] gives us the good source for reference. To justify the contact angle θ which is measured from the angle between the interface of an droplet and a liquid with respect to the membrane surface, we can use the analytical prediction for the critical pressure given by [62]:

$$\begin{aligned}\Delta P_c &= \frac{2\gamma\cos\theta}{a} \\ &\quad\times\sqrt[3]{1-\frac{2+3\cos\theta-\cos^3\theta}{4(R_0/a)^3\cos^3\theta-(2-3\sin\theta+\sin^3\theta)}},\end{aligned} \tag{2.53}$$

which is determined by the Young-Laplace pressure. In the limit $R_0 \to \infty$, the expression in Eq. 2.53 will converge to the critical pressure for an oil film on a membrane, which gives $\Delta P_c = 2\gamma\cos\theta/a$ [63]. We can also see clearly that the translocation time for the droplet becomes less when the pressure difference increases, as illustrated in Fig. 2.6.

At a given value of the pressure difference, the translocation time increasing as the initial size of the droplet R_0 increases are clearly seen in Fig. 2.7. We have chosen $R_0/a = 2.0, 2.5$ and 3.0 as representative values. For $R_0/a = 2.0$, we found that $\Delta P_c = 0.48\gamma/a$. Our results are in agreement with the results in [62] which are obtained from Eq. 2.53.

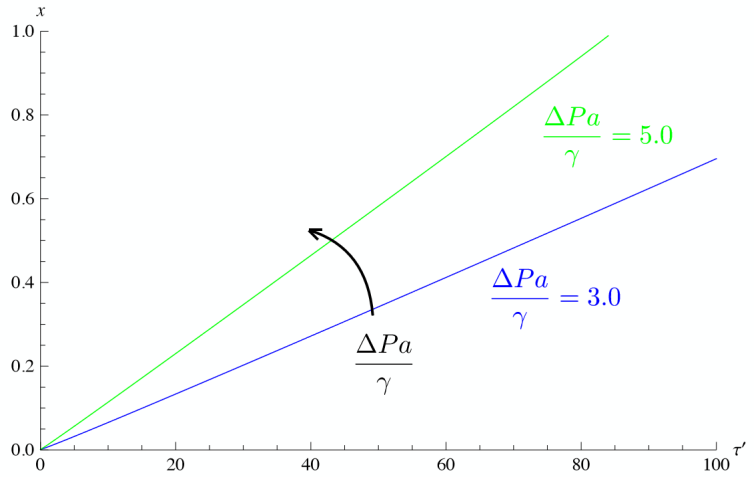

Figure 2.6: The evolution of the droplet at long time scale. At $R_0/a = 10.0$, our representative result shows clearly that the translocation time for the droplet decreases when the pressure difference increases.

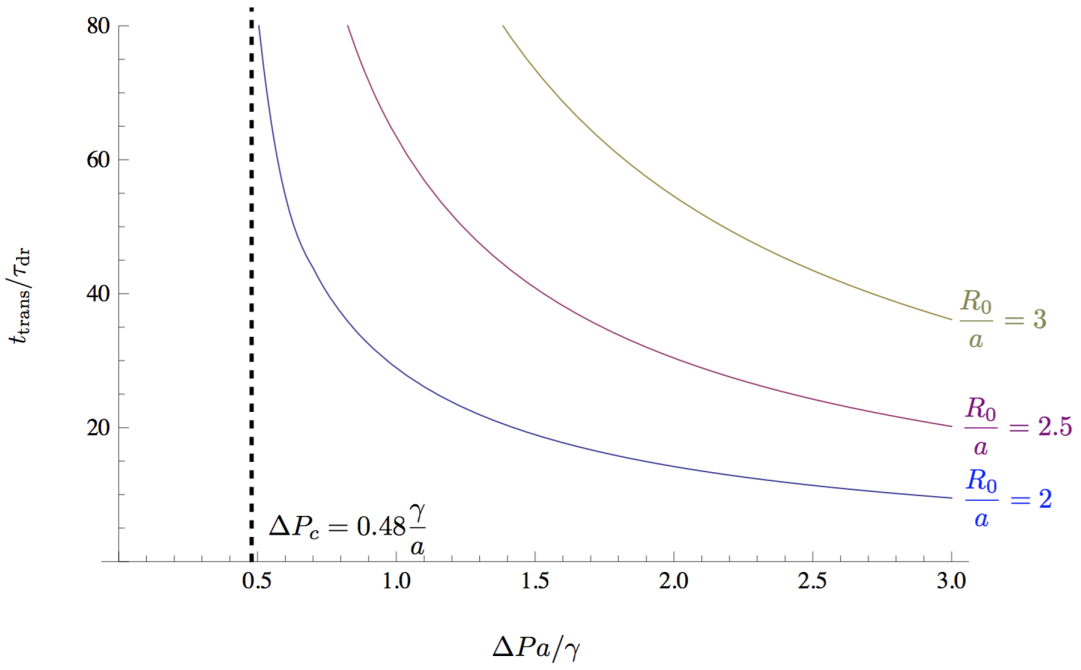

Figure 2.7: Translocation time of the droplet with different initial droplet's sizes is plotted as a function of the dimensionless variable $\Delta Pa/\gamma$. Inset: The critical pressure for the translocated droplet is plotted against the droplet's initial size.

C. Conclusions

We have used Onsager principle to investigate the translocation process of a droplet through a narrow hole across a membrane. The equation of motion for the droplet is derived by choosing the appropriate slow variables. Naturally, in the absence of any external driving force, the free energy landscape is symmetric around the translocation coordinate. Necessarily, the energy barrier decreases as the pressure gradient increases. The translocation time decreases as the pressure difference across the membrane increases, or the initial size of the droplet decreases as expected.

Apart from a droplet, study of translocation of a vesicle through a narrow hole across a membrane we need to take into account the effect of bilayer membranes of a vesicle. In order to to this, we need to introduce the concept of the Helfrich free energy. On a phenomenological level, including a potential asymmetry between the two monolayers constituting a bilayer membrane of a vesicle, the Helfrich free energy reads

$$F = \frac{\kappa}{2} \oint dA(2H - c_0)^2, \tag{2.54}$$

where κ is bending modulus of a vesicle membrane and A is the membrane area. H is the mean curvature which has dimensions of inverse length and c_0 is the spontaneous curvature arising from asymmetry in the areas of inner and outer membranes constituting a bilayer membrane of a vesicle.

CHAPTER III

The String Method

The kinetic pathways of the translocation are interesting to discuss. By solving the equation of motion obtained from the Onsager principle, the state changes of the vesicle can be described in the configuration space. On the other hand, the string method is a robust tool to obtain the reaction pathways [25], [26], [27]. The basic idea of the string method is to find a geodesic path between the initial and final states on the free energy surface. The condition that at each point on the paths the force perpendicular to the paths is zero gives the minimum energy paths (MEPs). In this chapter, we will discuss the string method used in our study. The concept and applications of the string method will be given in Secs 3.1 and 3.2.

3.1 The String Method for Computing the Minimum Energy Paths (MEPs)

The string method is a computational method for computing reaction paths or minimum energy paths (MEPs) for events that have energy barriers. Generally, the string methods are categorized into two types, i.e., (1) zero-temperature string method for computing MEPs on smooth energy landscapes and (2) finite-temperature string method for rough energy landscapes. Several computational methods are proposed for finding minimum energy paths [25], [26], [27], [28], [50], [51], [59]. Here we will discuss the concept of string method for computing MEPs on smooth energy landscapes in Sec. 3.1. The applications of the string method

will be shown through the representative free energy landscapes in Sec. 3.2.[1]

The basic idea of the string method is to evolve paths (strings) according to the potential force in the normal directions to the path on the free energy landscape. The condition that at each point on the paths the force perpendicular to the paths is zero gives the minimum energy paths (MEPs). In the string method, there are two steps, i.e., (i) evolution of the points on the initial guess string and (ii) interpolation of the string.

Let us consider the system described by the Langevin dynamics

$$\gamma\frac{dq}{dt} = -\nabla V(q) + \xi(t), \tag{3.1}$$

where γ is the friction coefficient. $\xi(t)$ is a Gaussian white noise with zero mean and satisfies the fluctuation-dissipation theorem

$$\langle \xi_j(t)\xi_k(0)\rangle = 2\gamma k_B T\delta_{jk}\delta(t), \tag{3.2}$$

where $\langle ...\rangle$ means the statistical average over the ensemble of noises. The metastable regions are localized around the minima of the potential $V(q)$ and MEP is the most probable transition pathway. Assuming that V has at least two minimal energy states, i.e., a and b which we want to find MEP connecting these two states. Let ψ be a path (string) connecting a and b (a and b can be considered as the initial and final states in the configuration space, respectively). By definition, ψ is MEP when the product between ψ and the force perpendicular to ψ must be zero, i.e.,

$$0 = (\nabla V)^{\perp}(\psi), \tag{3.3}$$

where $(\nabla V)^{\perp}$ is the component of (∇V) normal to ψ. For initial guess of the path, the force perpendicular to the path will be non-zero. We need to evolve the string according to the dynamics

$$u_n = -(\nabla V)^{\perp}(\psi), \tag{3.4}$$

[1]The original article about the applications of the string method for computing MEPs was accepted to publish in Thai Journal of Physics (in Thai) [53]. Here we give the English translation from the original article.

where u_n is the hypothetical normal velocity of the path. We can see clearly that Eq. 3.3 is the stationary state of Eq. 3.4.

In order to do numerical computations, we assume that the string is parametrized by α, i.e., $\psi = \{\varphi(\alpha), \alpha \in [0,1]\}$. The unit tangent vector of φ is defined by $\hat{\tau} = \varphi_\alpha/|\varphi_\alpha|$, where φ_α denotes the derivative of φ with respect to α. For simplicity, we use equal arc-length parametrization. In this case, we also have $|\varphi_\alpha| =$ const. Under this parametrization, Eq. 3.4 will be written as

$$\frac{\partial \varphi}{\partial t} = -(\nabla V)^{\perp}(\varphi) + \lambda\hat{\tau}, \tag{3.5}$$

where $\lambda\hat{\tau} = \lambda(\alpha, t)\hat{\tau}(\alpha, t)$ is a Lagrange multiplier added to enforce the parametrization. This Lagrange multiplier term does not affect the evolution of the string but it contributes the parametrization of the curve.

In order to find the MEP by using the string method, there are two steps:

Step 1: Evolution of the images

We discretize the initial guess string into set of images where

$$\varphi = \{\varphi_i(t),\ i = 0, 1, 2, ..., N\}. \tag{3.6}$$

We evolve the images within time step Δt through the equation

$$\frac{\partial \varphi_i}{\partial t} = -(\nabla V)^{\perp}(\varphi_i). \tag{3.7}$$

If we denote $\varphi_i^n, i = 0, 1, 2, ...N$ be the positions of the images after n iterations. After step 1, by using the Euler method, the new set of images is given by

$$\varphi_i^* = \varphi_i^n - (\Delta t)(\nabla V)^{\perp}(\varphi_i^n), \tag{3.8}$$

or by using the fourth order Runge-Kutta as

$$\varphi_i^* = \varphi_i^n - \frac{1}{6}k_i^{(1)} - \frac{1}{3}k_i^{(2)} - \frac{1}{3}k_i^{(3)} - \frac{1}{6}k_i^{(4)}, \tag{3.9}$$

where

$$\begin{aligned} k_i^{(1)} &= (\Delta t)(\nabla V)^{\perp}(\varphi_i^n), \\ k_i^{(2)} &= (\Delta t)(\nabla V)^{\perp}\Big(\varphi_i^n + \frac{1}{2}k_i^{(1)}\Big), \\ k_i^{(3)} &= (\Delta t)(\nabla V)^{\perp}\Big(\varphi_i^n + \frac{1}{2}k_i^{(2)}\Big), \\ k_i^{(4)} &= (\Delta t)(\nabla V)^{\perp}\Big(\varphi_i^n + k_i^{(3)}\Big). \end{aligned} \tag{3.10}$$

Step 2: Interpolation of the string

We would like to interpolate the points $\{\varphi_i^*\}$ on a nonuniform mesh $\{\alpha_i^*\}$ onto a uniform mesh where the number of points is preserved. We follow these two steps:

(1) We first calculate the arc length corresponding to φ_i^*. We define

$$s_0 = 0, \tag{3.11}$$

and

$$s_i = s_{i-1} + |\varphi_i^* - \varphi_{i-1}^*|, \quad i = 1, 2, 3, ..., N, \tag{3.12}$$

and mesh $\{\alpha_i^*\}$ can be obtained from normalizing $\{s_i\}$, i.e.,

$$\alpha_i^* = s_i / s_N \tag{3.13}$$

(2) We use the interpolation to obtain the points φ_i^{n+1} on uniform mesh $\alpha_i = i/N$ that can use, for example, cubic spline interpolation for $\{(\alpha_i^*, \varphi_i^*),\ i = 0, 1, 2, ..., N\}$ [54]. When the points $\{\varphi_i^{n+1},\ i = 0, 1, 2, ..., N\}$ are obtained, the process goes back to step 1 and iterates until convergence.

3.2 Applications for Computing MEPs

(i) We will first consider the two-dimensional potential energy for computing MEP by using the string method. The potential energy is written as

$$V(x, y) = (1 - x^2 - y^2)^2 + y^2/(x^2 + y^2). \tag{3.14}$$

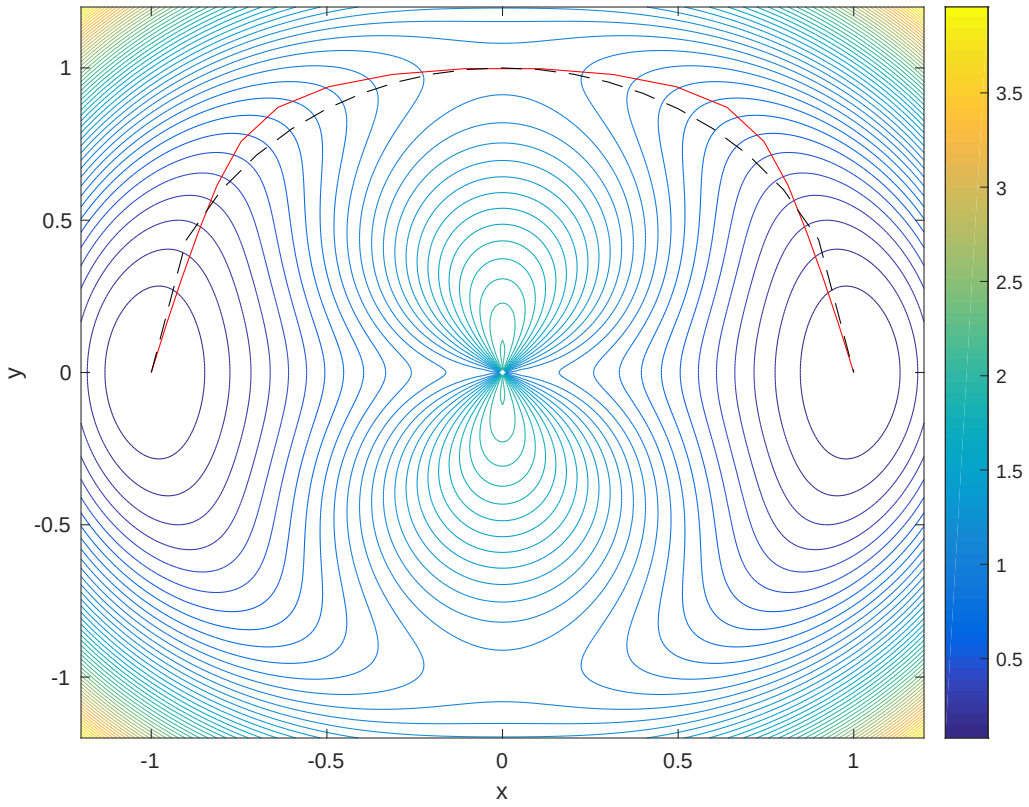

Figure 3.1: Contour line of the potential $V(x, y) = (1 - x^2 - y^2)^2 + y^2/(x^2 + y^2)$. We compare the minimum energy paths (MEPs) obtained from the string method (red solid curve) and the exact MEP (dashed black curve).

The contour line of the energy is illustrated in fig. 3.1. The minima are located at the points $(-1, 0)$ and $(1, 0)$, respectively. The exact minimum energy paths connecting these two states are the upper and lower part of the unit circle $x^2+y^2 = 1$.

In order to calculate MEPs we select the initial string which has the initial and final points at $(-1, 0)$ and $(1, 0)$, respectively. We discretize the string into $N = 20$ and use the forward Euler method, where $\Delta t = 2.5 \times 10^{-3}$ for evolving the string. The red solid curve in fig. 3.1 shows the calculated MEP compared to the exact MEP (dashed black curve). The error between the calculated and exact MEP might occur from (i) the number of point N is too small and (ii) the selected time step is inappropriate.

For the mth order accurate interpolation, the interpolation error is

interpolation error$= O(N^{-m})$,

where $m = 4$ for cubic spline scheme and the error for evolving points on the string scales as

evolution error$= O(\Delta t^{-l})$,

where $l = 2$ for the Euler method.

(ii) The Müller-Brown potential

The Müller-Brown potential energy is often used for testing algorithms for finding transition pathways and minimum energy paths. The analytic form of the potential is given by [55]

$$V(x, y) = \sum_{k=1}^{4} A_k \exp\left[a_k(x - x_k^0)^2 + b_k(x - x_k^0)(y - y_k^0) + c_k(y - y_k^0)^2\right], \quad (3.15)$$

where

$A = (-200, -100, -170, 15)$,

$a = (-1, -1, -6.5, 0.7)$,

$b = (0, 0, 11, 0.6)$,

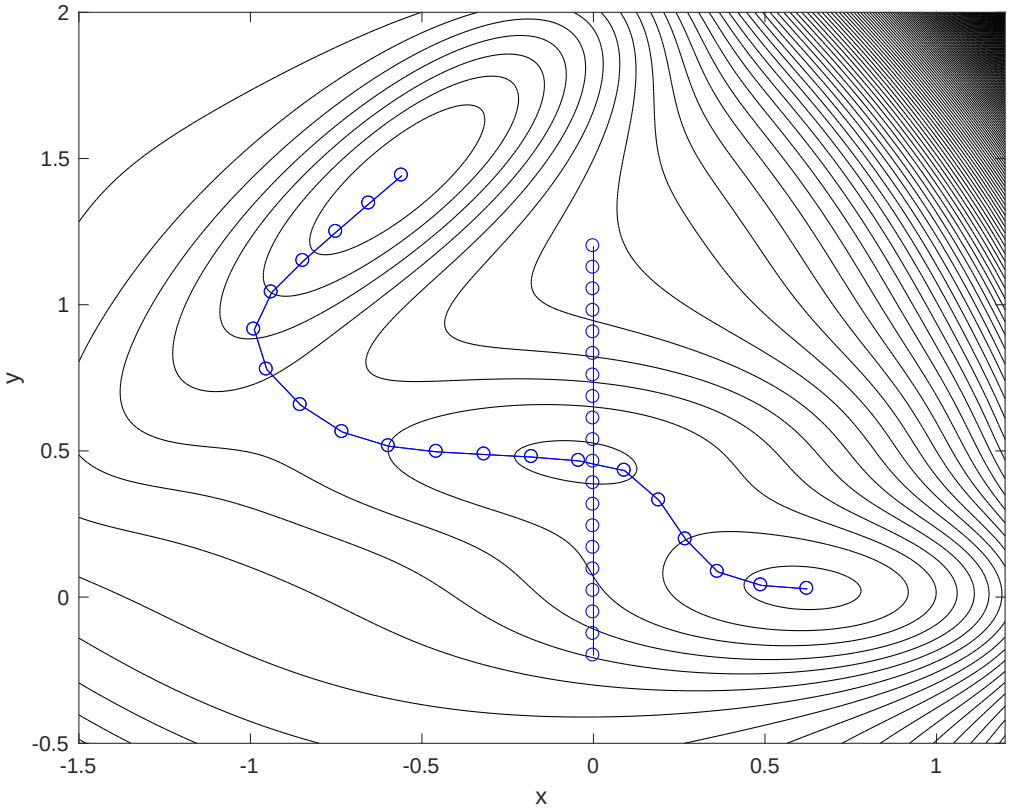

Figure 3.2: The initial string (the vertical line) and the calculated MEP (the other one) on the Müller-Brown potential. The initial string is discretized into 20 points. The Euler method is used for evolving the points on the string. The number of iterations is $n = 2,000$.

$$c = (-10, -10, -6.5, 0.7),$$

$$x^0 = (1, 0, -0.5, -1),$$

$$y^0 = (0, 0.5, 1.5, 1).$$

The Müller-Brown potential has three minima and two saddle points. For finding MEP, we discretize the initial string into $N = 20$ connecting the points $(0, -0.25)$ and $(0, 1.25)$ as in Fig. 3.2. We use Euler method for evolving the points on the string with $n = 2,000$ for the number of iterations. Fig. 3.2 shows the initial guess string (vertical line) and the other one is calculated MEP.

CHAPTER IV

Translocation of a Vesicle Through a Narrow Hole Across a Membrane

We discuss translocation of a vesicle through a hole across a membrane, where we focus on the kinetic pathway of the translocation in this chapter. The free energy and the dissipation function of the system are given. The vesicle's evolution equations are also shown in Sec. 4.1. Section 4.2 is devoted for results and discussions of the study. The emergence of the free energy barriers associated with the pressure difference is discussed. We investigate the reaction paths obtained from the string method and the actual kinetic paths obtained from the Onsager principle when the friction between the surfactant molecules and the surface membrane is changed. Our results show that those paths are significantly different from each other when the pressure gradient is large [29]. We also show clearly that the translocation time of the vesicle decreases as the pressure difference increases, or the initial size decreases. We end this chapter with conclusion of the study in Sec. 4.3.

4.1 Theory of a Vesicle

The shape of a translocating vesicle is modeled by two connected spheres as illustrated schematically in Fig. 4.1. The translocating vesicle has radii $r_1(t)$ and $r_2(t)$, where $r_1(t)$ and $r_2(t)$ stand for the radii of the lower and upper parts of

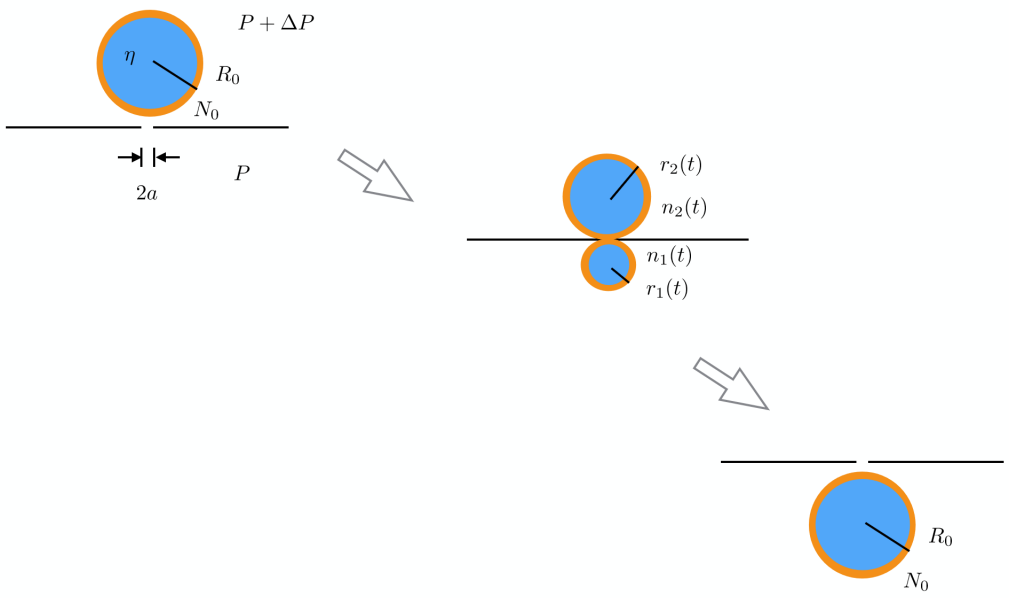

Figure 4.1: Model of a translocating vesicle.

the vesicle, respectively. Furthermore, the number of surfactant molecules on the enclosed surfaces with radii $r_1(t)$ and $r_2(t)$ is denoted by $n_1(t)$ and $n_2(t)$, respectively. We neglect the thickness of the membrane of the vesicle. The vesicle is assumed to be initially a sphere of radius R_0 consisting of N_0 surfactant molecules. R_0 is assumed to be much larger than the size of the narrow hole on the membrane and the thickness of the membrane is assumed to be negligible. Then we can neglect the structure of the hole and we regard the hole as a circle with radius a. The pressure is almost constant in the upper (and the lower) part of the vesicle, but drops significantly across the hole connecting the two parts. The pressure difference between inside and outside of the spherical vesicle is determined by the Laplace pressure. The liquid inside the vesicle is assumed to be incompressible with viscosity η. Most of the energy dissipation is taking place at the hole when the membrane and the liquid are going through, where the translocation velocity is also assumed to be small.

Now we construct a dynamical equation for our model system. If we have a set of slow variables $\mathbf{x} = (x_1, x_2, ..., x_f)$, Onsager principle is described by the

minimization of Rayleighian defined by

$$R = \Phi + \dot{A}, \tag{4.1}$$

with respect to $\dot{x_i}$, where Φ is the energy dissipation function and $\dot{A}$ is the time derivative of the free energy.

We have chosen $r_1(t)$, $r_2(t)$, $n_1(t)$ and $n_2(t)$ as the slow variables of the translocating vesicle. We can further reduce the degrees of freedom to two by using the volume conservation $R_0^3 = r_1^3 + r_2^3$ together with the conservation of the total number of molecules $N_0 = n_1 + n_2$. By letting ϕ as a surfactant number density, where ϕ is defined by (the number of surfactant molecules)/(surface area), the second constraint can be rewritten as $\phi_0 R_0^2 = \phi_1 r_1^2 + \phi_2 r_2^2$, where $\phi_0 = N_0/4\pi R_0^2$, $\phi_1 = n_1/4\pi r_1^2$ and $\phi_2 = n_2/4\pi r_2^2$, respectively. To understand how the translocation time of the vesicle depends on the initial size R_0 as well as the pressure difference ΔP, we introduce dimensionless parameters a/R_0 and $\Delta P a/\lambda$, where λ is the stretching modulus of the stretched membrane constituting the vesicle.

4.1.1 The Potential Energy

We have assumed that, at equilibrium, the vesicle with surface area $S_0 = 4\pi R_0^2$ has a number of surfactant molecules N_0. Then, if we stretch out the vesicle to two connected spheres with surface areas S_1 and S_2, their surface area differences compared to their equilibrium surface areas should be written as $4\pi(r_1^2 - R_0^2(n_1/N_0))$ and $4\pi(r_2^2 - R_0^2(1 - n_1/N_0))$ for the lower and upper parts in Fig. 4.1, respectively. Then, the stretching energy of the membrane takes the form

$$A = \frac{1}{2}\lambda 4\pi \frac{\left(r_1^2 - R_0^2\left(\frac{n_1}{N_0}\right)\right)^2}{R_0^2\left(\frac{n_1}{N_0}\right)} + \frac{1}{2}\lambda 4\pi \frac{\left(r_2^2 - R_0^2\left(1 - \left(\frac{n_1}{N_0}\right)\right)\right)^2}{R_0^2\left(1 - \left(\frac{n_1}{N_0}\right)\right)} - \Delta P \frac{4\pi}{3}(r_1^3 - r_2^3), \tag{4.2}$$

where the bending elastic energy is constant for a spherical vesicle and we have neglected its contribution. We rewrite Eq. 4.2 in terms of the dimensionless variables

x and y, where x and y are defined by

$$x = \left(\frac{r_1}{R_0}\right)^3, \tag{4.3}$$

and

$$y = \frac{n_1}{N_0} = \frac{\phi_1}{\phi_0} \cdot \left(\frac{r_1}{R_0}\right)^2, \tag{4.4}$$

respectively. Then, the energy is rewritten as

$$\begin{aligned} A\left(x, y; \frac{a}{R_0}; \frac{\Delta P a}{\lambda}\right) &= a^2\lambda\left\{2\pi\left(\frac{R_0}{a}\right)^2\left[\frac{(x^{2/3}-y)^2}{y} + \frac{((1-x)^{2/3}-(1-y))^2}{1-y}\right]\right. \\ &\quad \left. -\frac{4\pi}{3}\left(\frac{R_0}{a}\right)^3\left(\frac{\Delta P a}{\lambda}\right)(2x-1)\right\}. \end{aligned} \tag{4.5}$$

4.1.2 The Energy Dissipation Function

The energy dissipation is caused mostly at the hole. It arises not only from the moving liquid but also from the moving surfactant molecules. In the limit of small Reynolds number, the dissipation function for the vesicle is given by

$$\Phi = \frac{1}{2}\zeta_s a v_s^2 + \frac{1}{2}\zeta_l a^2 (v_s - v_l)^2, \tag{4.6}$$

where ζ_s represents the friction coefficient of the hole on the surfactant molecules, and ζ_l is related to the viscosity. Generally, the friction coefficients should be functions of the slow variables and they can be derived from the Stokesian hydrodynamics. In this work, however, for the sake of simplicity, they are assumed to be constants. Note that ζ_s and ζ_l have the units of kg m^{-1} s^{-1}, and kg m^{-2} s^{-1}, respectively. The surfactant velocity v_s and the liquid flow velocity v_l are defined by

$$v_s = \frac{\dot{n}_1}{\pi a(\phi_1 + \phi_2)} = \frac{4(r_1 r_2)^2 \dot{n}_1}{a(n_1 r_2^2 + n_2 r_1^2)}, \tag{4.7}$$

and

$$v_l = \frac{\dot{V}_1}{\pi a^2} = \left(\frac{2r_1}{a}\right)^2 \dot{r}_1, \tag{4.8}$$

respectively. The first term in Eq. 4.6 is caused from the membrane through the friction force against the moving surfactant molecules, while the second term is the dissipating energy caused by the relative motion of the liquid and the surfactant molecules. By introducing the dimensionless parameter, $\zeta_s/\zeta_l a$, the energy dissipation function for the vesicle can be rewritten from Eqs. 4.6, 4.7 and 4.8 as

$$\begin{aligned}\Phi\left(\dot{x},\dot{y};\frac{a}{R_0};\frac{\zeta_s}{\zeta_l a}\right) &= 8a^4\zeta_l\left(\frac{R_0}{a}\right)^4\left\{\left(\frac{R_0}{3a}\right)^2\dot{x}^2\right. \\ &+\left(1+\frac{\zeta_s}{\zeta_l a}\right)\frac{x^{4/3}(1-x)^{4/3}}{[(1-x)^{2/3}y+(1-y)x^{2/3}]^2}\dot{y}^2 \\ &\left.-\left(\frac{2R_0}{3a}\right)\frac{x^{2/3}(1-x)^{2/3}}{[(1-x)^{2/3}y+(1-y)x^{2/3}]}\dot{x}\dot{y}\right\}. \qquad (4.9)\end{aligned}$$

4.1.3 The Vesicle's Evolution Equations

By minimizing the vesicle Rayleighian $R = \Phi + \dot{A}$ with respect to $\dot{x}$ and $\dot{y}$, we obtain the two-coupled differential equations

$$\begin{aligned}\frac{dx}{dt'} &= -\frac{9}{32}\left(\frac{a}{R_0}\right)^7\left(1+\frac{\zeta_l a}{\zeta_s}\right)f(x,y) \\ &-\frac{3}{32}\left(\frac{a}{R_0}\right)^6\left(\frac{\zeta_l a}{\zeta_s}\right)\left[\frac{y}{x^{2/3}}+\frac{(1-y)}{(1-x)^{2/3}}\right]g(x,y), \qquad (4.10)\end{aligned}$$

and

$$\begin{aligned}\frac{dy}{dt'} &= -\frac{1}{32}\left(\frac{a}{R_0}\right)^5\left(\frac{\zeta_l a}{\zeta_s}\right)\left[\frac{y}{x^{2/3}}+\frac{(1-y)}{(1-x)^{2/3}}\right] \\ &\times\left\{\left(\frac{3a}{R_0}\right)f(x,y)+\left[\frac{y}{x^{2/3}}+\frac{(1-y)}{(1-x)^{2/3}}\right]g(x,y)\right\}, \qquad (4.11)\end{aligned}$$

where we have defined

$$\begin{aligned}f(x,y) &= 2\pi\left(\frac{R_0}{a}\right)^2\left[\frac{4}{3}(x^{2/3}-y)\frac{x^{-1/3}}{y}-\frac{4}{3}((1-x)^{2/3}-(1-y))\frac{(1-x)^{-1/3}}{(1-y)}\right] \\ &-\frac{8\pi}{3}\left(\frac{R_0}{a}\right)^3\left(\frac{\Delta P a}{\lambda}\right), \qquad (4.12)\end{aligned}$$

and

$$g(x,y) = 2\pi\left(\frac{R_0}{a}\right)^2\left[-\frac{(x^{4/3}-y^2)}{y^2}+\frac{(1-x)^{4/3}-(1-y)^2}{(1-y)^2}\right]. \tag{4.13}$$

The dimensionless time t' is defined by $t' = t/\tau$, where $\tau = \zeta_l a^3/2R_0\lambda$. We have assumed that, at the initial state, the lower part of the vesicle is a sphere with radius a and its surfactant density is $(\phi_1)_{\rm i}$. This gives $x(t'=0) = (a/R_0)^3$ and the initial condition for y is $y(t'=0) = [(\phi_1)_{\rm i}/\phi_0](a/R_0)^2$.

4.2 Results and Discussions

4.2.1 Energy Barrier

Figure 4.2 shows the free energy landscape of the translocating vesicle for $R_0/a = 2.0$, where the horizontal and vertical axes stand for the dimensionless variables x and y, respectively. In the absence of the pressure difference across the membrane, the energy landscape is symmetric with respect to $(x,y) = (0.5, 0.5)$ as illustrated in Fig. 4.2 (a). We can see clearly that the free energy barrier moves from the midpoint toward the initial point along the trajectory as the pressure difference increases, as shown in Fig. 4.2 (from (a) to (b)). Moreover, it disappears when $\Delta P a/\lambda \geq 0.05$ as illustrated in Figs. 4.2 (c) and (d). Our results suggest a decreasing in the energy barrier as the pressure difference increases. It should be noted that a similar free energy landscape was studied by Shojaei *et al.* [22] In their consideration, the pore volume is also taken into account. In contrast, we neglect such detailed structure of the pore in order to highlight the qualitative behavior of the kinetic pathway.

In the work of Shojaei *et al.* [22], the energy for the vesicle shape is described by a bending modulus κ_c and a stretching modulus λ through the form:

$$F = \frac{1}{2}\kappa_c \oint dA(2H - c_0)^2 + \frac{1}{2A_0}\lambda(\Delta A)^2, \tag{4.14}$$

where the mean curvature H is defined by $H \equiv (1/R_1 + 1/R_2)/2$. ($R_1$ and R_2 stand for the radii of principal curvatures.) c_0 is the spontaneous curvature, and

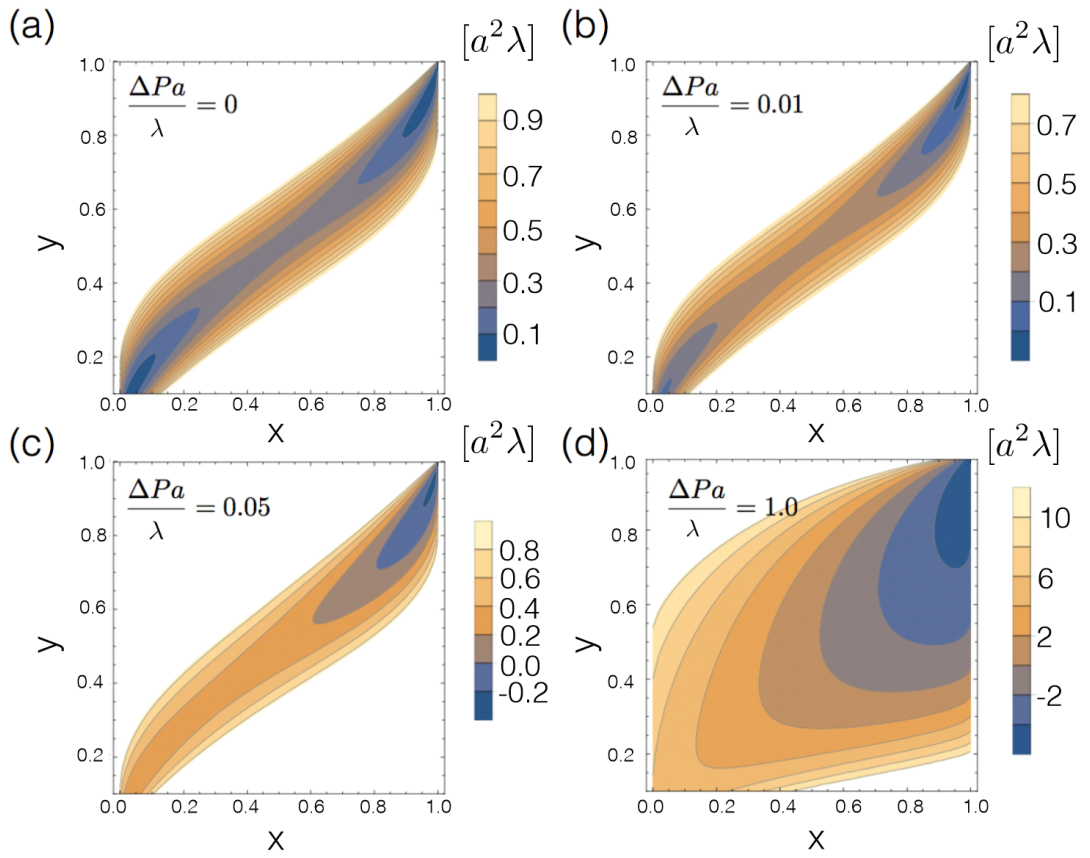

Figure 4.2: Free energy landscape with $\Delta Pa/\lambda = 0.0, 0.01, 0.05$ and 1.0 at $R_0/a = 2.0$. The horizontal and vertical axes refer to the dimensionless variables x and y, respectively.

ΔA is the change in the total area of the vesicle, which is defined by $\Delta A = A - A_0$, where A_0 is the area of the initial vesicle and A is that of the stretched vesicle. In the absence of any external driving force, their representative results show the decreasing in the energy barrier as the spontaneous curvature increases. The effect is obviously noticed when the vesicle is being at the crossing stage (The stage that the partial vesicle occupies the volume of the pore, while its remainder is partitioned into both sides of the pore. In the consideration of Shojaei *et al*. [22], the pore has a cylindrical shape.). The symmetry in the free energy landscape in the absence of any external driving force is found naturally in our results and in ref. [22] In the presence of the external potential difference, Shojaei *et al*. [22] reported the effect of changing the bending and the stretching moduli on the free energy landscape, when the vesicle has no spontaneous curvature c_0. Their results suggest that variation of the bending modulus affects the energy barrier significantly, while the variation of the stretching modulus seems to affect the barrier insignificantly.

4.2.2 Reaction Path and Kinetic Path

The reaction path is the path of the state change which is usually identified with the minimum energy path (MEP), whose shape can be obtained by the string method. Generally, the string method is used for computing the MEP in configuration space. If the MEP is a path φ connecting two states a and b, i.e. two endpoints of the string on the free energy landscape A, then, by definition, φ must satisfy

$$(\nabla A)^{\perp}(\varphi) = 0, \tag{4.15}$$

where $(\nabla A)^{\perp}$ is the component of (∇A) normal to φ. Once the free energy A is obtained (Eq. 4.5), we can directly get the reaction path from Eq. 4.15. Our initial trial string is discretized into a set of points where each point corresponds to different states and morphologies of the system. For such initial guess of the path, the force perpendicular to the path will be non-zero. We need to evolve the

string according to the dynamics

$$-(\nabla A)^{\perp}(\varphi) = u_n, \tag{4.16}$$

where u_n is the hypothetical normal velocity of the path. We can see clearly that Eq. 4.15 is the stationary state of Eq. 4.16. Generally, kinetic path which is the actual kinetic pathway can be significantly different from reaction path since reaction path is determined by the free energy $A(x, y)$ only while kinetic path depends also on kinetic coefficients (ζ_s and ζ_l). In the following results, we will show the comparison between the reaction paths obtained from the string method and the actual kinetic paths obtained from the Onsager principle when $\zeta_s/\zeta_l a$ is changed on the free energy landscape.

At $R_0 = 10.0a$ and $\Delta Pa = 0.02\lambda$, Fig. 4.3 shows that the reaction path (blue line with filled circle) is slightly different from the kinetic paths. The difference can be seen clearly when $\Delta Pa = \lambda$ in Fig. 4.4.

Figures 4.3 and 4.4 indicate that reaction and kinetic paths are close to each other if the external force on the liquid flow is small (and this is independent of the kinetic coefficients), while they are significantly different from each other if the external force is large. Because the external force exerted on the liquid flow induces a quick flow of the liquid compared to the diffusion of the surfactant molecules, the time evolution of x is much faster than the evolution of y. This is why we have the difference between the result from the string method and the kinetic paths obtained from the Onsager principle.

In the limit that ζ_s is very large, the surfactant distribution (the change of y) changes very slowly, while the liquid transport (the change of x) takes place very quickly. In this case, we may assume that y is the slow variable, and x is in equilibrium for given y, i.e. $\partial A/\partial x = h(x, y) = 0$. This determines the kinetic path for large value of ζ_s as shown in Figs. 4.3 and 4.4 with solid red lines. The state variables (x, y) will quickly approach to the kinetic path, and then moves slowly along the kinetic path. The translocation time is determined by the dynamics of y along the kinetic path.

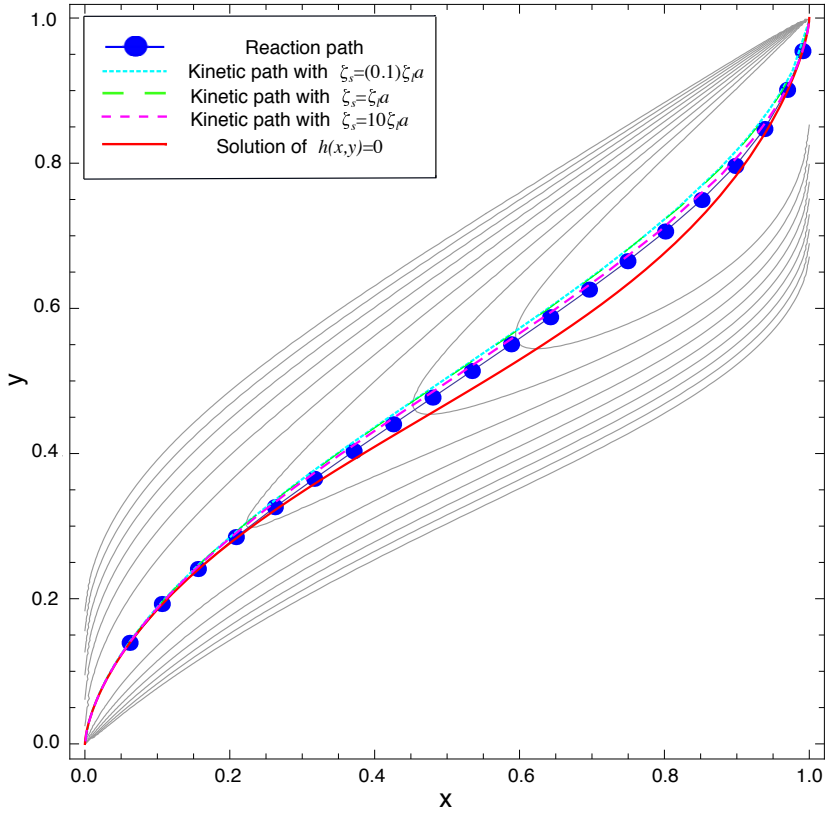

Figure 4.3: Free energy landscape at small external force. The reaction and the kinetic paths are evaluated at $R_0 = 10.0a$ with $\Delta Pa = 0.02\lambda$. The free energy landscape has a steep valley for $\zeta_s/\zeta_l a = 0.1, 1.0$, and 10.0. The initial string is discretized into 20 points. The solid red line indicates the kinetic path for large value of ζ_s.

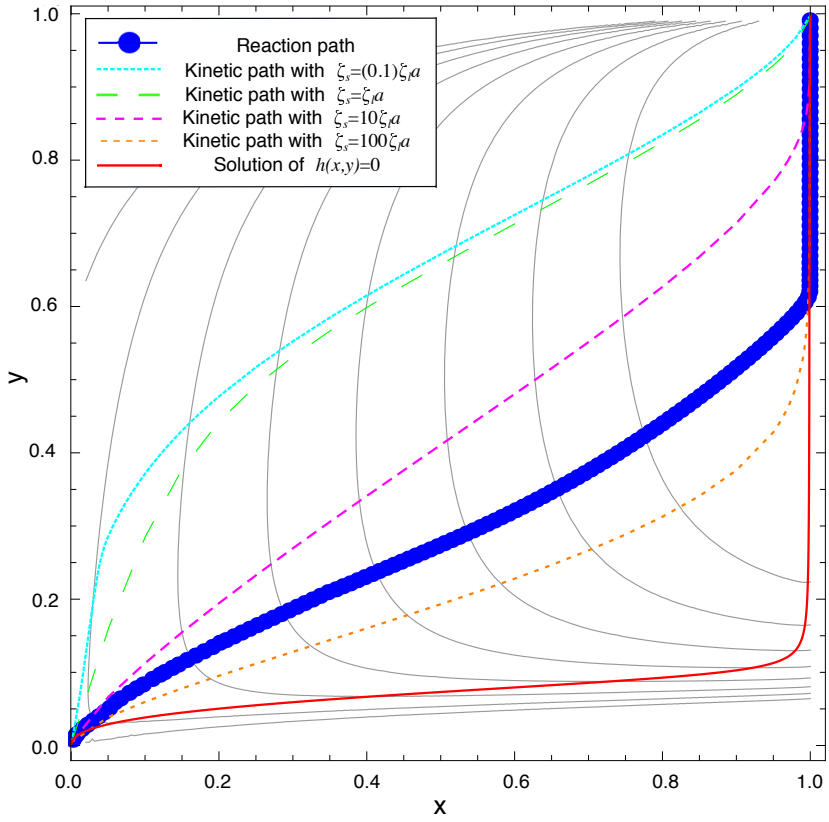

Figure 4.4: Free energy landscape at large external force. The free energy landscape becomes flatter for $\Delta Pa = \lambda$. We give the results with $\zeta_s/\zeta_l a = 0.1, 1.0, 10.0$ and 100.0. The initial string is discretized into 150 points.

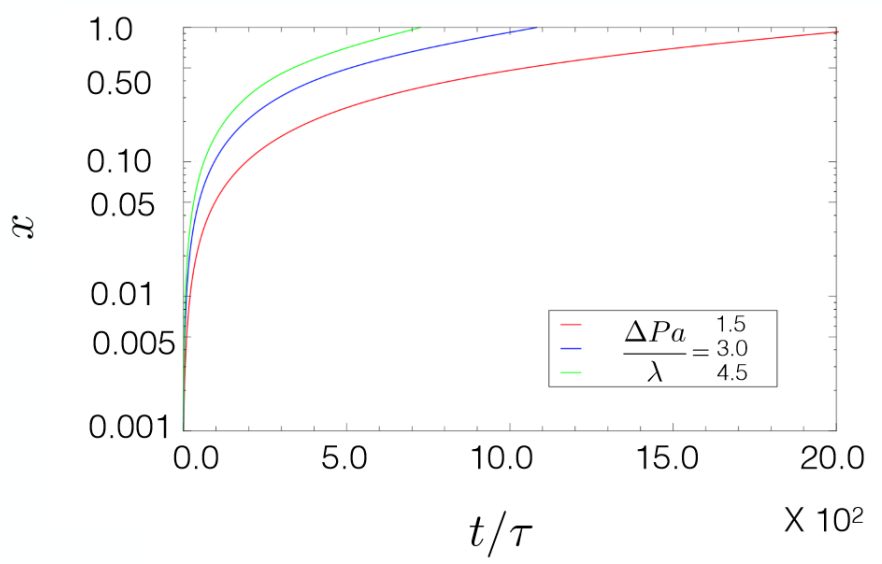

Figure 4.5: The time evolution of the vesicle. At $R_0/a = 10.0$ and $\zeta_s = 2\zeta_l a$, we give the results for the translocating vesicle with different values of the pressure difference across the membrane. The horizontal axis is defined by $t' = 2R_0\lambda t/\zeta_l a^3$, where λ and ζ_l are the stretching modulus and the friction coefficient related to the viscosity of the fluid inside the vesicle, respectively. The vertical axis is defined by $x = (r_1/R_0)^3$.

4.2.3 Translocation Time

To clearly understand the effect of the friction coefficient ζ_s on the translocation time of the vesicle, we have considered a system which has small and large values of ζ_s at $R_0/a = 10.0$ and the initial surfactant density is chosen as $(\phi_1)_{\rm i} = 0.5\phi_0$. For the case of small ζ_s, we have chosen $\zeta_s = 2\zeta_l a$. On the other hand, $\zeta_s = 1,000\zeta_l a$ holds for the case of large ζ_s. We see clearly that the translocation time decreases when the pressure difference increases and, at the same value of ΔP, the vesicle has succeeded in the translocating with less translocation time for the small value of ζ_s. The results are shown in Figs. 4.5 and 4.6.

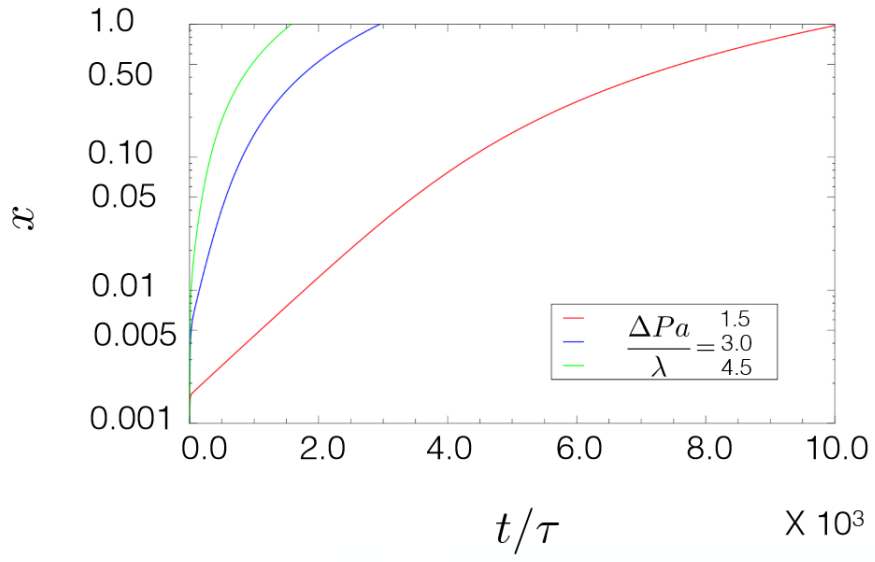

Figure 4.6: The motion of the vesicle with the different pressure gradient at $\zeta_s = 1,000\zeta_l a$. The initial size of the vesicle is set as $R_0 = 10.0\,a$. The initial surfactant density is chosen as $(\phi_1)_{\rm i} = 0.5\phi_0$.

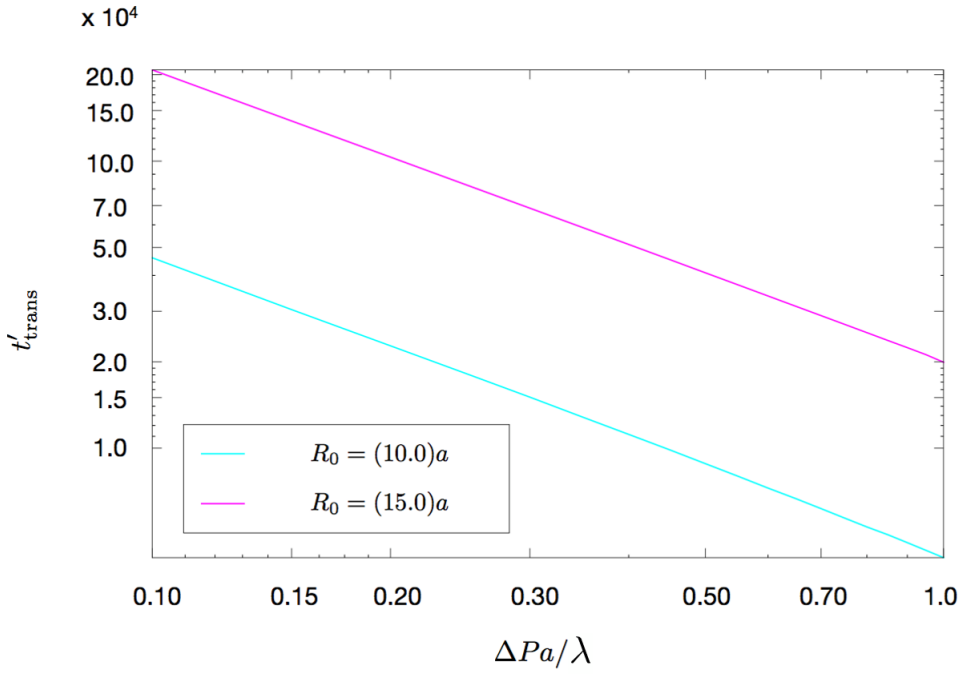

Figure 4.7: Translocation time of the vesicle with different its initial size is plotted as a function of the dimensionless variable $\Delta Pa/\lambda$. The graphs are evaluated at $\zeta_s = 10\zeta_l a$, $(\phi_1)_{\text{i}} = 0.5\phi_0$.

The translocation time of the vesicle is plotted against $\Delta Pa/\lambda$ as illustrated in Fig. 4.7 at $\zeta_s = 10\zeta_l a$. The translocation time increases as the initial size of the vesicle R_0 increases at a given value of the pressure difference. The authors in ref. [22] have considered the effect of various parameters on the translocation time by using the Fokker-Planck formalism. For each vesicle size, their results suggested that the translocation time decreases as the external driving force increases as in our results. At a given constant external driving force, their results showed that the effect of the stretching modulus λ (the last term in Eq. 4.14) on the translocation time is weaker than the bending modulus κ_c (the first term in Eq. 4.14). In our model, we use non-dimensional equations, where the behavior of the model is specified by a few numbers of non-dimensional parameters. Thus, we do not have to change individual parameters such as λ and κ_c as they did in ref. [22]. We should change only the two parameters i.e. $\Delta Pa/\lambda$ and R_0/a.

4.3 Conclusions

We have used Onsager principle to investigate the translocation process of a vesicle through a narrow hole across a membrane. The equations of motion for the translocating vesicle are derived by choosing the appropriate slow variables. The potential energy is calculated by considering the stretching energy of the translocating vesicle and the pressure difference across the membrane. There is a free energy barrier for translocation process of a vesicle through a narrow hole due to stretching of the vesicle. In the absence of the pressure difference, the free energy landscape is symmetric around the translocation coordinate and its magnitude depends on the initial size of the vesicle. The height of the barrier can be decreased by applying the pressure gradient across the membrane. By increasing the pressure difference or decreasing the initial size of the vesicle, the translocation time becomes shorter.

The kinetic paths obtained from the Onsager principle are independent of the friction coefficients ζ_s and ζ_l when the pressure difference is small and those

paths are close to the reaction paths (the minimum energy paths) obtained from the string method. On the other hand, they are significantly different from each other if the pressure difference is large. Because the pressure exerted on the liquid flow induces a quick flow of the liquid compared to the diffusion of the surfactant molecules, the diffusion flow of the liquid volume inside the vesicle (denoted by the variable x) is much faster than the migration of the number of the surfactant molecules (denoted by the variable y). This is the reason why we have the difference between the result from the string method and the kinetic paths obtained from the Onsager principle. This means that we have already shown that Onsager principle is an extension of the conventional string method when the external driving force is large.

In our model, we have considered the hole on a rigid membrane wall as a circular hole with fixed radius a. However, in real physical system e.g. translocation of a white blood cell through a hole on blood vessel wall (transcellular diapedesis), pore can change its size during the translocation process. In such a case, our model needs to be extended by introducing one more variable i.e. size of the pore. In the present work, however, we neglected such a degree of freedom, and predicted the dependencies of translocation kinetics of a single vesicle on its stretching property and size and on the applied pressure difference. We hope that our simple model would stimulate experiments on the study of translocation of vesicle through a narrow hole.

CHAPTER V

Birthing of a Daughter Vesicle in Self-reproducing Vesicle System

Recently, Sakuma and Imai [38] established a temperature-controlled cyclic self-reproducing vesicle system without feeding. The characteristic feature of their system is that the vesicle composed of cylinder-shaped lipids [1, 2-dipalmitoyl-*sn*-glycero-3-phospho choline (DPPC)] and inverse-cone-shaped lipids [1, 2-dilauroyl-*sn*-glycero-3-phos phoethanolamine (DLPE)]. The vesicle forms an inclusion vesicle called daughter vesicle inside the mother vesicle and then the daughter vesicle is expelled through the small pore on the mother vesicle. In this chapter we present theoretical model on the birthing process of a single, rigid daughter vesicle through a pore. By using a simple geometric picture, we derive the free energy constituting the material properties of the mother vesicle, i.e., bending, stretching and line tension moduli, as functions of the distance between centers of the daughter and mother vesicles. We see clearly the disappearance of the energy barrier by selecting appropriate moduli. The dynamics of the system is studied by employing the Onsager principle. The results indicate that translocation time decreases as the friction parameter decreases, or the initial size of the daughter vesicle decreases.

We organize this chapter as follows. In Sec. 5.1, we describe the theory for a birthing daughter vesicle. Section 5.2 is devoted to the discussion of the results of the birthing vesicle. We end this chapter with the conclusion of this study in Sec 5.3.

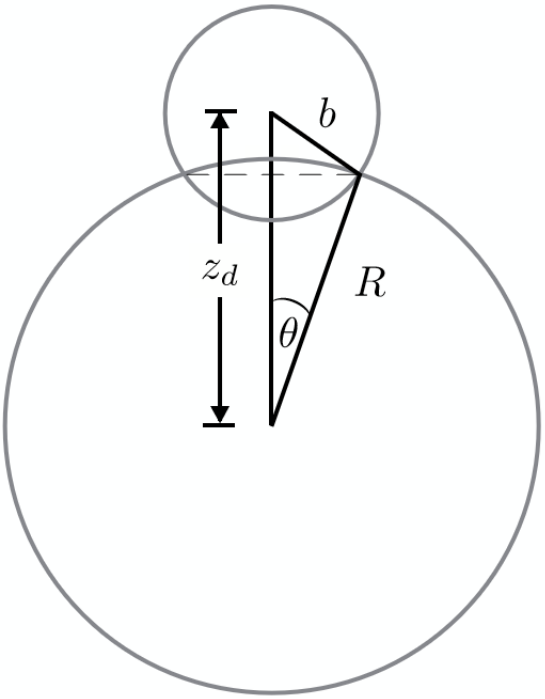

Figure 5.1: Model of a birthing daughter vesicle.

5.1 Theory of a Birthing Vesicle

5.1.1 Geometry

The birthing of a single, spherical, rigid daughter vesicle with radius b through a pore of the spherical mother vesicle with radius R is modeled by a simple geometric ansatz as illustrated in Fig. 5.1. We neglect the thickness of the membrane of the mother vesicle. The distance between the centers of the mother and daughter vesicles is denoted by z_d. During the birthing process, the pore on the surface of

the mother vesicle gradually expand and shrink due to line tension energy. We have assumed that the pore has a circular shape with radius a where its center is located on the straight line between the centers of the mother and daughter vesicles. The angle defined by the line joining the centers of the mother and daughter vesicles, and the line between the center of the mother vesicle and the edge of the hole is denoted by θ. At initial state, the daughter vesicle is a little bit expelled from the mother vesicle which has radius R_0. The distance and angle at the initial state are denoted by $z_{d,0}$ and θ_0, respectively. When the daughter vesicle is completely expelled from the mother vesicle and the pore is completely closed, we will have $\theta = 0$. Then, θ has a maximum value when the daughter vesicle passes the mother vesicle with half of its volume. Investigation of Fig. 5.1. shows that the three variables R, z_d, and θ are related with each other by the geometry of constraint

$$\cos\theta = \frac{R^2 + z_d^2 - b^2}{2 z_d R}. \tag{5.1}$$

It follows that we may take z_d as the only one independent variable that describes the system. We assume that during the birthing process there is no water goes out from the mother vesicle and the daughter vesicle moves very slowly. Then, the volume of the mother vesicle is conserved.

5.1.2 The Potential Energy

We have assumed that, at equilibrium, the mother vesicle has a spherical shape. The potential energy is composed of the bending, stretching and line tension energies,

$$F = \frac{\kappa}{2}\int dA(2H - c_0)^2 + \frac{\lambda}{2}\frac{(A - A_{\rm eq})^2}{A_{\rm eq}} + \sigma \oint dl, \tag{5.2}$$

where κ, λ, and σ are bending, stretching, and line tension moduli, respectively.

The first term on the right hand side of Eq. 5.2 is the bending energy which is harmonic in the mean curvature H, where H is defined by $H \equiv (1/R_1 + 1/R_2)/2$. ($R_1$ and R_2 stand for the radii of principal curvatures.) c_0 is the spontaneous curvature. Typically, the bending modulus κ is of the order of 10 $k_B T$. The

experimental techniques to measure this bending modulus and its reported values are given in [58].

The second term on the right hand side of Eq. 5.2 shows the stretching energy of the mother vesicle. It is in the form of harmonic in the change of vesicle surface area $A - A_{\rm eq}$, where $A_{\rm eq} = 4\pi R_{\rm eq}^2$ which is the equilibrium surface area of the mother vesicle and A is the mother vesicle surface area subtracted by the area of the pore, which is determined by R and θ. The value of the stretching modulus λ is taken in the order of $10^{-1}\, k_B T/\mu\mathrm{m}^2$.

The last term on the right hand side of Eq. 5.2 refers to the line tension energy of the system which is proportional to the total length of the pore. Experimentally, it is rather difficult to measure the line tension modulus σ of the membrane constituting DPPC and DLPE directly. In our study, we will give a prediction for the value of σ which is assumed to be of the order of $1\, k_B T/\mu\mathrm{m}$.

We can analytically calculate the bending, stretching, and line tension energies of the system based on the differential geometry of the curved surface. First, let us calculate the contribution to the free energy from the bending. The Helfrich free energy is given by

$$F_b = \frac{\kappa}{2} \int dA (2H - c_0)^2. \tag{5.3}$$

The integral $\int dA$ is taken over the area $A_{\text{mother vesicle}} - A_{\text{pore}} = 2\pi R^2 (1 + \cos\theta)$. Then, this bending energy reduces to

$$F_b = \pi \kappa R^2 (1 + \cos\theta) \left(\frac{2}{R} - c_0 \right)^2, \tag{5.4}$$

where we have used $H = 1/R$ for the spherical mother vesicle with radius R and the spontaneous curvature is c_0. Using Eq. 5.1, we can eliminate $\cos\theta$ and, then, we obtain the Helfrich free energy in terms of the parameters R, z_d, and b as

$$F_b = \pi \kappa R^2 \left(1 + \frac{R^2 + z_d^2 - b^2}{2 z_d R} \right) \left(\frac{2}{R} - c_0 \right)^2. \tag{5.5}$$

In order to obtain the stretching energy, we first calculate square of the

change in the surface area of the mother vesicle as

$$\begin{aligned}(\Delta A)^2 &= (A - A_{\rm eq})^2 \\ &= [(A_{\text{mother vesicle}} - A_{\rm pore}) - A_{\rm eq}]^2 \\ &= [2\pi R^2(1+\cos\theta) - 4\pi R_{\rm eq}^2]^2. \end{aligned} \tag{5.6}$$

Then, the stretching energy is

$$\begin{aligned}F_s &= \frac{\lambda}{2}\frac{(\Delta A)^2}{A_{\rm eq}} \\ &= \frac{\pi\lambda}{2R_{\rm eq}^2}[R^2(1+\cos\theta) - 2R_{\rm eq}^2]^2 \\ &= \frac{\pi\lambda}{2R_{\rm eq}^2}\left[R^2\left(1+\frac{R^2+z_d^2-b^2}{2z_dR}\right) - 2R_{\rm eq}^2\right]^2, \end{aligned} \tag{5.7}$$

where the law of cosine Eq. 5.1 comes to the end for eliminating θ.

Likewise, we calculate the line tension energy. It is given by

$$F_l = 2\pi\sigma R\sin\theta. \tag{5.8}$$

Since $\cos\theta = (R^2+z_d^2-b^2)/(2z_dR)$, from the identity $\sin^2\theta + \cos^2\theta = 1$, we easily obtain

$$\sin\theta = \sqrt{1 - \frac{(R^2+z_d^2-b^2)^2}{(2z_dR)^2}}. \tag{5.9}$$

Then, the line tension energy becomes

$$F_l = 2\pi\sigma R\sqrt{1 - \frac{(R^2+z_d^2-b^2)^2}{(2z_dR)^2}}. \tag{5.10}$$

The total free energy of the system as a function of the radius R, the distance z_d, and the radius of the daughter vesicle b is

$$\begin{aligned}F[R, z_d; b] &= \pi\kappa R^2\left(1+\frac{R^2+z_d^2-b^2}{2z_dR}\right)\left(\frac{2}{R} - c_0\right)^2 \\ &\quad + \frac{\pi\lambda}{2R_{\rm eq}^2}\left[R^2\left(1+\frac{R^2+z_d^2-b^2}{2z_dR}\right) - 2R_{\rm eq}^2\right]^2 \\ &\quad + 2\pi\sigma R\sqrt{1 - \frac{(R^2+z_d^2-b^2)^2}{(2z_dR)^2}}. \end{aligned} \tag{5.11}$$

Here we should note that R is not independent of z_d. We have assumed that during the birthing process the volume of the mother vesicle is preserved. So, R can be determined by the constraint

$$\begin{aligned}\Delta V &= \frac{4}{3}\pi R^3 - \pi b^2\Big[(R\cos\theta - z_d) + b\Big] \\ &\quad + \frac{\pi}{3}\Big[(R\cos\theta - z_d)^3 + b^3\Big] \\ &\quad - \pi R^3(1-\cos\theta) + \frac{\pi R^3}{3}(1-\cos^3\theta) \\ &\quad - \frac{4}{3}\pi R_0^3 + \pi b^2\Big[(R_0\cos\theta_0 - z_{d,0}) + b\Big] \\ &\quad - \frac{\pi}{3}\Big[(R_0\cos\theta_0 - z_{d,0})^3 + b^3\Big] \\ &\quad + \pi R_0^3(1-\cos\theta_0) - \frac{\pi R_0^3}{3}(1-\cos^3\theta_0) \\ &= 0, \end{aligned} \tag{5.12}$$

together with Eq. 5.1. Then, the free energy Eq. 5.11 is a function of z_d and b only.

5.1.3 The Energy Dissipation Function

When the daughter vesicle is moving through the pore, the energy dissipation is caused mostly at the pore. In the limit of small Reynolds number, the dissipation function for the daughter vesicle is given by

$$\Phi = \frac{1}{2}\zeta \dot{z_d}^2, \tag{5.13}$$

where ζ is the friction coefficient. Generally, the friction coefficient is a function of the slow variables and it can be derived from the Stokesian hydrodynamics. In this work, we assume that the friction coefficient is proportional to the radius of the pore a and can be written as

$$\begin{aligned}\zeta &= 2\pi\alpha a \\ &= 2\pi\alpha R\sin\theta, \end{aligned} \tag{5.14}$$

where α is related to the viscosity of the fluid and has the unit of kg m^{-1} s^{-1}.

5.1.4 The Equation of Motion

The Rayleighian of the system is

$$\begin{aligned} R &= \Phi + \dot{F} \\ &= \frac{1}{2}\zeta \dot{z_d}^2 + \frac{dF(z_d)}{dt} \\ &= \frac{1}{2}\zeta \dot{z_d}^2 + \frac{\partial F}{\partial z_d}\dot{z_d}. \end{aligned} \tag{5.15}$$

By minimizing R with respect to $\dot{z_d}$, i.e., $\partial R/\partial \dot{z_d} = 0$, we obtain the equation of motion for the daughter vesicle

$$\dot{z_d} = -\frac{1}{\zeta}\frac{\partial F}{\partial z_d}. \tag{5.16}$$

5.2 Results and Discussions

We present our results by first discussing the explicit free energy landscapes when the bending, stretching, and line tension moduli are changed. We then show the effect of adding water into the mother vesicle on the energy barrier. The kinetics of birthing will be discussed when the friction coefficient is changed or the size of the daughter vesicle is varied.

5.2.1 Free Energy Landscapes

A representative results of the free energy landscapes over z_d when the bending, stretching, and line tension moduli change are shown in Figs. 5.2, 5.3, and 5.4.

All plots in Figs. 5.2, 5.3, and 5.4 are evaluated when the size of the daughter vesicle is fixed at $b = 10\,\mu$m, while the equilibrium size of the mother vesicle is $R_{\rm eq} = 30\,\mu$m. The initial size of the mother vesicle is $R_0 = 40\,\mu$m. The spontaneous curvature c_0 is set to zero.

Figure 5.2 shows the increasing of the free energy when the bending modulus κ increases while the stretching and line tension moduli are fixed at $\lambda =$

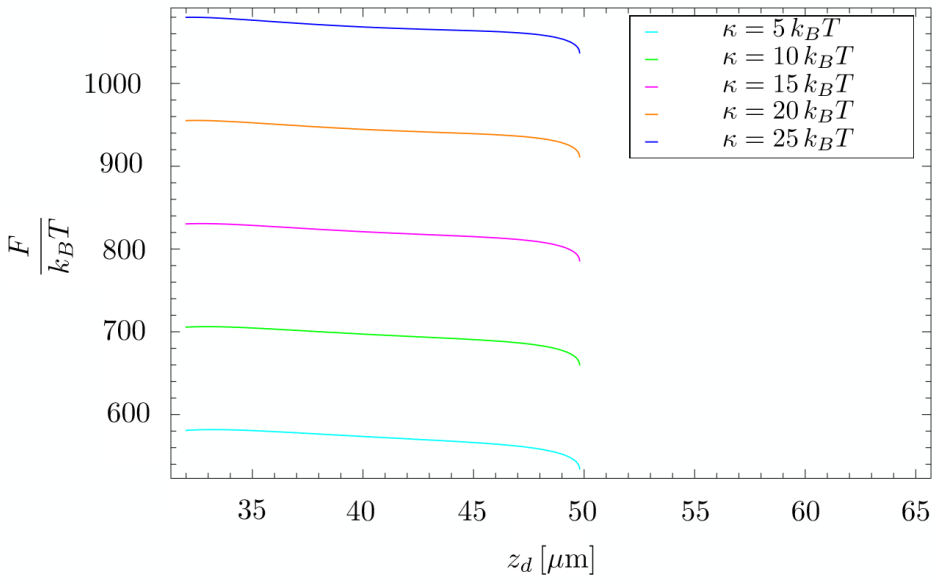

Figure 5.2: The free energy landscapes when the bending modulus κ increases. The stretching and line tension moduli are fixed at $\lambda = 0.125\,k_BT/\mu\mathrm{m}^2$ and $\sigma = 1.0\,k_BT/\mu\mathrm{m}$, respectively. The size of the daughter vesicle is $b = 10\,\mu\mathrm{m}$, while the equilibrium size of the mother vesicle is $R_{\mathrm{eq}} = 30\,\mu\mathrm{m}$. The initial size of the mother vesicle is $R_0 = 40\,\mu\mathrm{m}$. The spontaneous curvature $c_0 = 0$.

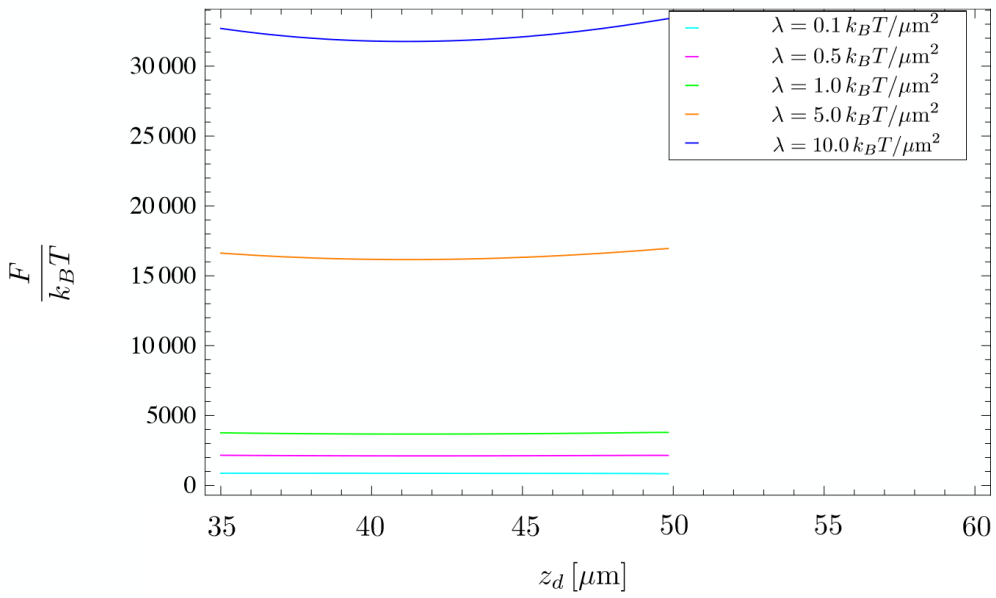

Figure 5.3: The free energy landscapes with the variation of the stretching modulus λ. The bending and line tension moduli are fixed at $\kappa = 20\,k_BT$ and $\sigma = 1.0\,k_BT/\mu$m, respectively. The other parameters are the same as those in Fig. 5.2.

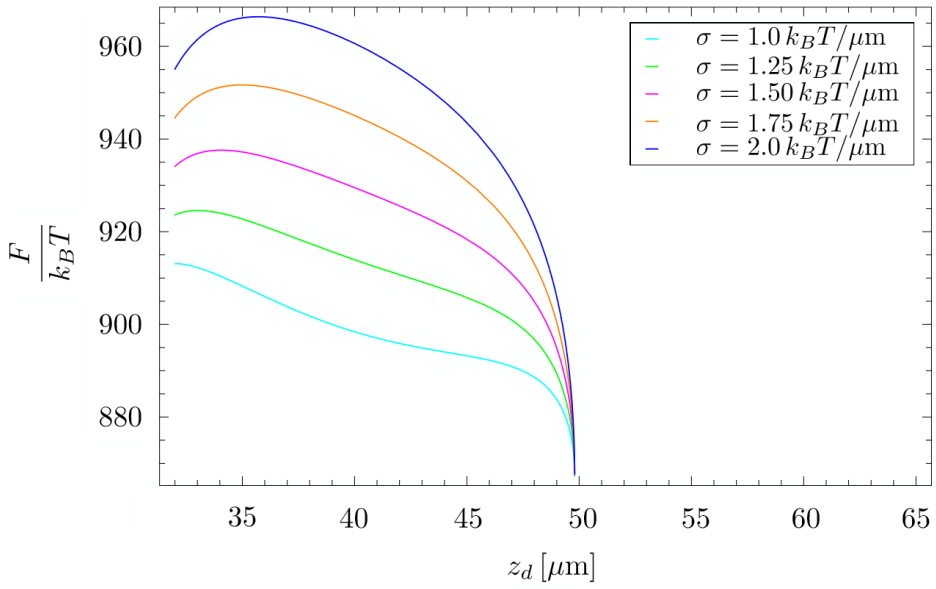

Figure 5.4: The free energy landscapes with changing of the line tension modulus σ. The bending and stretching moduli are fixed at $\kappa = 15\,k_BT$ and $\lambda = 0.15\,k_BT/\mu\mathrm{m}^2$, respectively. b is fixed at $10\,\mu\mathrm{m}$. $R_{\mathrm{eq}} = 30\,\mu\mathrm{m}$, $R_0 = 40\,\mu\mathrm{m}$, and $c_0 = 0$.

$0.125\,k_BT/\mu\text{m}^2$ and $\sigma = 1.0\,k_BT/\mu\text{m}$, respectively. All graphs show that there is no energy barrier and the daughter vesicle succeeds in the birthing process at $z_d < 50\,\mu\text{m}$. This means that the size of the mother vesicle is reduced from its initial size. This effect will be seen clearly when the daughter vesicle is large compare to the size of the mother vesicle.

Figure 5.3 shows the effect of varying the stretching modulus on the free energy landscape. In this figure, the bending and line tension moduli are fixed at $\kappa = 20\,k_BT$ and $\sigma = 1.0\,k_BT/\mu\text{m}$, respectively. We can see clearly that there is a metastable state at $\lambda = 10.0\,k_BT/\mu\text{m}^2$ which means the daughter vesicle is trapped. The depth of this metastable state can be decreased by decreasing the stretching modulus.

The free energy landscapes when the line tension modulus σ changes are shown in Fig. 5.4. The bending and stretching moduli are fixed at $\kappa = 15\,k_BT$ and $\lambda = 0.15\,k_BT/\mu\text{m}^2$, respectively. We see clearly the decreasing in the energy barrier when σ decreases. The daughter vesicle has succeeded in the birthing at $\sigma = 1.0\,k_BT/\mu\text{m}$ when the energy barrier disappears.

The effect of adding water into the mother vesicle is shown in Fig. 5.5, where $\kappa = 20\,k_BT$, $\lambda = 0.125\,k_BT/\mu\text{m}^2$, and $\sigma = 2.75\,k_BT/\mu\text{m}$. Due to water supplying, the initial size of the mother vesicle is changed and we select $R_0 = 40, 50, 60$, and $70\,\mu\text{m}$. We see the decreasing of the energy barrier and existence of the metastable state, where the daughter vesicle stops moving at $R_0 = 70\,\mu\text{m}$. The highest value of the free energy is also increasing when the pressure inside the mother vesicle increases due to adding more water.

5.2.2 Kinetics of Birthing

The free energy landscapes when $\kappa = 15\,k_BT$, $\lambda = 0.170\,k_BT/\mu\text{m}^2$, and $\sigma = 1.0\,k_BT/\mu\text{m}$ is used to verify the kinetic of the birthing process at $T = 35°\text{C}$. By solving Eq. 5.16 numerically, we obtain the trajectory of the daughter vesicle when the friction coefficient is changed as shown in Fig.5.6, The result shows clearly

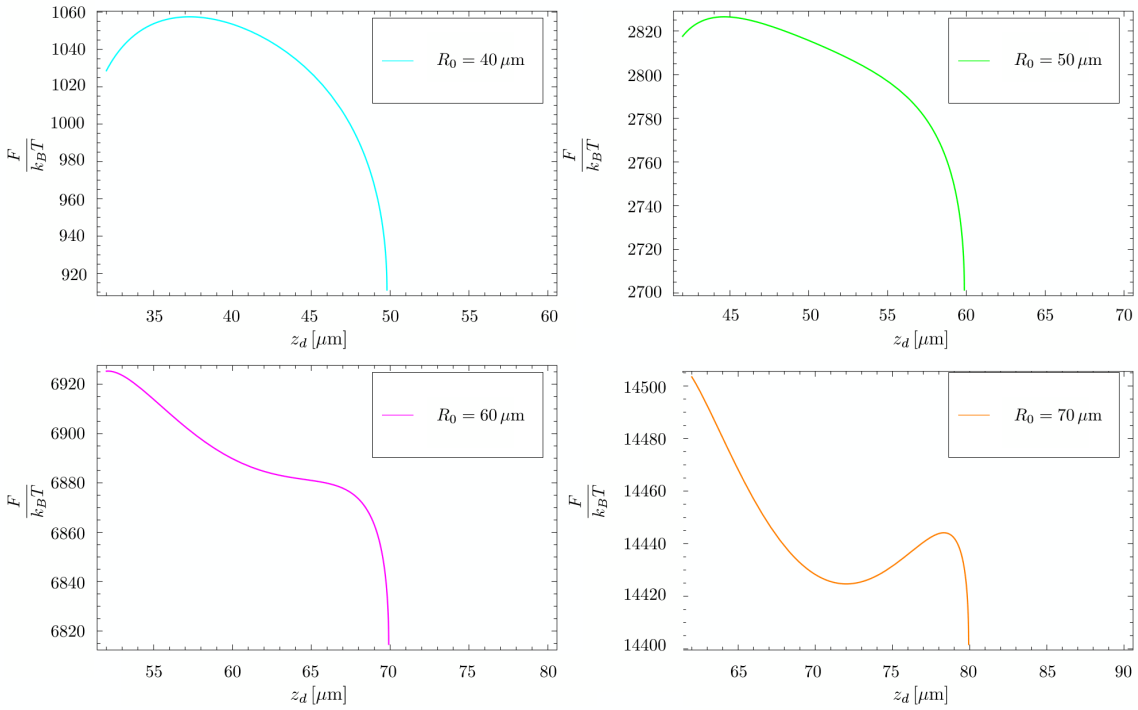

Figure 5.5: The free energy landscapes with the variation of R_0. The bending, stretching, and line tension moduli are fixed at $\kappa = 20\,k_BT$, $\lambda = 0.125\,k_BT/\mu\text{m}^2$, and $\sigma = 2.75\,k_BT/\mu\text{m}$, respectively. b is fixed at $10\,\mu$m, $R_{\text{eq}} = 30\,\mu$m, and $c_0 = 0$.

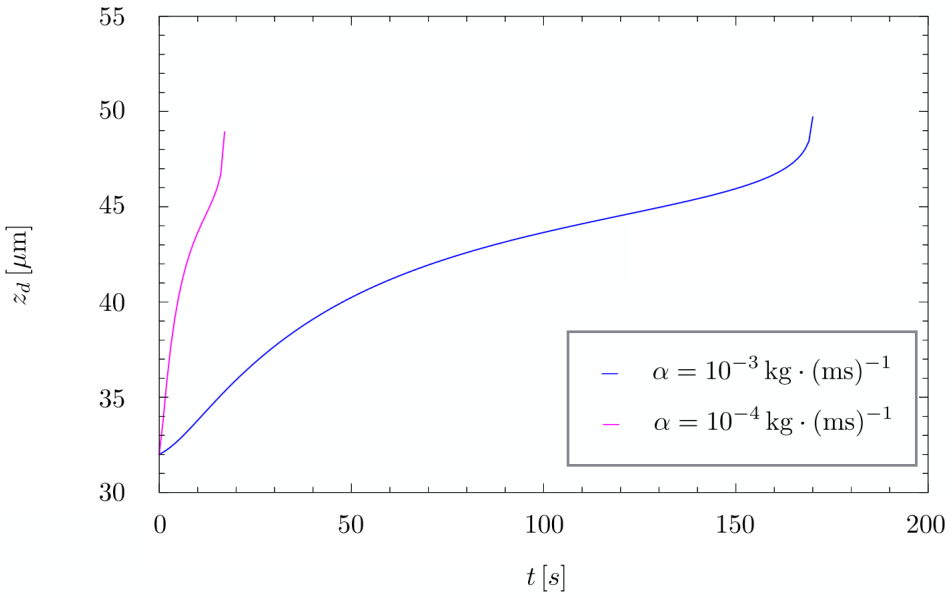

Figure 5.6: The motion of the daughter vesicle with different value of the friction coefficient. The bending, stretching, and line tension moduli are fixed at $\kappa = 15\,k_BT$, $\lambda = 0.170\,k_BT/\mu\mathrm{m}^2$, and $\sigma = 1.0\,k_BT/\mu\mathrm{m}$, respectively. The results are evaluated at $T = 35°\mathrm{C}$. $b = 10\,\mu\mathrm{m}$, $R_{\mathrm{eq}} = 30\,\mu\mathrm{m}$, $R_0 = 40\,\mu\mathrm{m}$, and $c_0 = 0$.

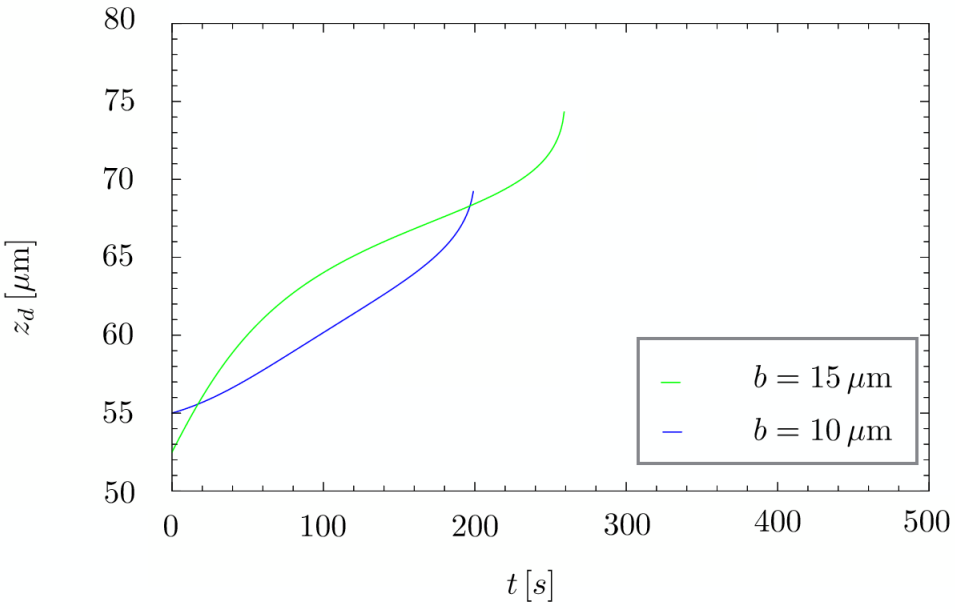

Figure 5.7: The trajectory of the daughter vesicle with different size b. The bending, stretching, and line tension moduli are fixed at $\kappa = 20\,k_BT$, $\lambda = 0.110\,k_BT/\mu\mathrm{m}^2$, and $\sigma = 1.5\,k_BT/\mu\mathrm{m}$, respectively. The friction coefficient is fixed at $\zeta = 10^{-7}\,\mathrm{kg}\cdot\mathrm{s}^{-1}$ The results are evaluated at $T = 35°\mathrm{C}$. $R_{\mathrm{eq}} = 40\,\mu\mathrm{m}$, $R_0 = 60\,\mu\mathrm{m}$, and $c_0 = 0$.

that the daughter vesicle has succeeded in the birthing with less translocation time when the friction is small.

At $R_{\mathrm{eq}} = 40\,\mu\mathrm{m}$ and $R_0 = 60\,\mu\mathrm{m}$, Fig. 5.7 shows the trajectory of the daughter vesicle with different size b, when $\kappa = 20\,k_BT$, $\lambda = 0.110\,k_BT/\mu\mathrm{m}^2$, and $\sigma = 1.5\,k_BT/\mu\mathrm{m}$ are kept constant. The friction coefficient is fixed at $\zeta = 10^{-7}\,\mathrm{kg}\cdot\mathrm{s}^{-1}$ and $T = 35°\mathrm{C}$. The result indicates that, for a big daughter vesicle, the mother vesicle feels more uncomfortable. Then the big daughter vesicle is expelled with high velocity compared to the small daughter vesicle. However, the velocity is reduced due to the barrier from line tension energy. Finally, it can escape from the mother vesicle with high velocity again.

5.3 Conclusions

We have used a simple geometric ansatz to study the birthing of the daughter vesicle in self-reproducing vesicle system. Onsager principle is used to derive the equation of motion for the birthing vesicle in terms of the bending, stretching and line tension moduli of the mother vesicle, and the size of the daughter vesicle, and the distance between the centers of the daughter and mother vesicles. The deformation of the mother vesicle is treated within the Helfrich free energy formalism and the stretching energy plays a role as a driving force for the system.

The derived free energy suggested that changing the stretching and line tension moduli affects the free energy landscapes clearly, while changing the bending modulus does not affect much the energy landscapes. This suggested that the system is mainly governed by the competition between the stretching and line tension energies. Adding more water into the mother vesicle will give an increase in the free energy and a decrease in the energy barrier. Because of the competition between the stretching and line tension energies, adding water up to some certain amount causes the dip in the free energy landscape. Further adding more water, the metastable state occurs which means the daughter vesicle is trapped and the birthing process is not completed. The translocation time decreases when the friction caused by the hole against the motion of the daughter vesicle decreases. Our results also suggest that when the daughter vesicle is large, the mother vesicle feels more uncomfortable. Consequently, the large daughter vesicle is then expelled with higher speed compared to the case of small daughter vesicle. However, the high speed will be decreased by the effect of barrier from the line tension energy.

In our model, the specific details regarding the chemical properties of the vesicle are parametrized in terms of the material parameters such as bending, stretching, and line tension moduli for the purpose of investigating the large scale properties of the birthing process. From the experimental point of view, measuring the bending, stretching, and line tension moduli of the membrane directly is rather

difficult. However, experimentalists could compare their experimental data to our predicted results to estimate the value of the moduli.

CHAPTER VI

Conclusions

In this thesis, we have examined the dynamics of translocation of a vesicle through a narrow pore by using Onsager variational principle. The problems of interest are translocation of a vesicle through a narrow hole across a membrane and birthing of a daughter vesicle in self-reproducing vesicle system. We will summarize and conclude the study as follows.

The first chapter is an introduction of the thesis. We state the remarkably flexible surfaces of vesicles, which show an interesting variety of shape deformations. Our first example of a vesicle shape deformation is budding transition. A series of images of L-α-dimyristoylphosphatidylcholine (DMPC) bilayer vesicle in pure water at different temperatures are shown. The vesicle shows shape deformations from a simple spherical shape at the lowest temperature to the budding state when the temperature is increased. Another example of observed shape change when the temperature is being increased is transitions from discocyte to inside budded shape via stomatocyte of a DMPC vesicle in pure water.

A brief historical development of the study of translocation of a vesicle through a small hole due to external driving forces is given. Many attempts tried to answer the question how the effectiveness of such filtration process depends on various parameters of the system such as the driving forces, bending and stretching moduli of the vesicle, the initial size of the vesicle, and geometry and size of the pore. Apart from the previous studies, we focus on the kinetic pathway of the translocating vesicle. We employ the string method to investigate the reaction paths of the kinetic. Those path are compared to the kinetic paths obtained from

the Onsager principle.

Another problem of such translocation process is the birthing of a vesicle through a pore in self-reproducing vesicle system. In our study, we theoretically model the birthing process of the daughter vesicle. We, again, employ the Onsager principle to investigate kinetic of the system. The chapter ends with the outline of this thesis.

In Chapter 2, Onsager variational principle which is the physical theory we use in this thesis, is explained in details. We take the problem in hydrodynamics, i.e., the dynamics of particle-fluid systems to describe the principle. Small particles moving in viscous fluids, e.g., particles sedimenting in a fluid can be described by the force balance between the potential force and the frictional force.

We first discuss a particle moving in a viscous fluid and calculate the friction constant for a spherical rigid particle. Considering motion of particles in viscous fluids, Rayleigh defined the dissipation function which allowed us to write the potential dissipation in analogous with potential force. We then define the Rayleighian of the system which is a sum of dissipation function and time derivative of the potential energy. We can see that the force balance between the potential force and the frictional force is equivalent to the minimization of Rayleighian over the rate of change of the coordinate of the system. It is the competition between dissipation and rate of change of the energy. Onsager noticed that many phenomenological equations describing the time evolution of the non-equilibrium systems are written in the form of particle-fluid system. He then proved that the reciprocal relation must hold for such a kind of the time evolution equation. This casts the evolution law of such systems into a variational principle called the Onsager variational principle which bases on the existence of slow variables. We give an example of application of Onsager principle to study translocation of a droplet through a narrow hole across a membrane.

The kinetic pathways of the translocation are interesting to discuss. By solving the equation of motion obtained from the Onsager principle, the state changes of the vesicle can be obtained on the configuration space. On the other

hand, the string method is a robust tool to obtain the reaction pathways. We discuss the string method and give some examples of its application in Chapter 3.

In Chapter 4, we discuss translocation of a vesicle through a hole across a membrane, where we focus on the kinetic pathway of the translocation. The free energy and the dissipation function of the system are derived. The vesicle's evolution equations are shown. The emergence of the free energy barriers associated with the pressure difference is discussed. We investigate the reaction paths obtained from the string method and the actual kinetic paths obtained from the Onsager principle when the friction between the surfactant molecules and the surface membrane is changed. Our results show that those paths are significantly different from each other when the pressure difference across the membrane is large. We also show clearly that the translocation time of the vesicle decreases as the pressure difference increases, or the initial size decreases.

Chapter 5 is devoted to theoretical study to describe experimental results done by Sakuma and Imai [38]. In this chapter we present theoretical model on the birthing process of a single, rigid daughter vesicle through a pore. On the mother vesicle, by using a simple geometric consideration, we derive the free energy constituting the material properties of the mother vesicle, i.e., bending, stretching and line tension moduli, as functions of the distance between centers of the daughter and mother vesicles. We see clearly the disappearance of the energy barrier by selecting appropriate moduli. The dynamics of the system is studied by employing the Onsager principle. The results indicate that the translocation time decreases as the friction parameter decreases, or the initial size of the daughter vesicle decreases.

References

[1] Y. Sakuma and M. Imai, Life **5**, 651 (2015).

[2] D. W. Deamer and J. P. Dworkin, Top. Curr. Chem. **259**, 1 (2005).

[3] P. Walde, Orig. Life Evol. Biosph. **36**, 109 (2006).

[4] J. N. Israelachvli, *Intermolecular and Surface Forces* (Academic Press, 1992).

[5] S. A. Safran, *Statistical Thermodynamics of Surfaces, Interfaces, and Membranes* (Addison-Wesley, 1994).

[6] U. Seifert, Adv. Phys. **46**, 13 (1997).

[7] D. Nelson, T. Piran, and S. Weinberg, *Statistical Mechanics of Membranes and Surfaces* (World Scientific Publishing, 2004).

[8] J. K̈as and E. Sackmann, Biophys. J. **60**, 825 (1991).

[9] K. Berndl, J. K̈as, R. LIpowsky, E. Sackman, and U. Seifert, Europhys. Lett., **13**, 659 (1990).

[10] P. B. Canham, J. theoret. Biol. **26**, 61 (1970).

[11] W. Helfrich, Z. Naturforsch. C **28**, 693 (1973).

[12] E. Evans, Biophys. J. **14**, 923 (1974).

[13] M. M. Mezei and V. Gulasekharam, Life Sci. **26**, 1473 (1980).

[14] C. Wachter, U. Vierl and G. Cevc, J. Drug. Targeting **16**, 611 (2008).

[15] D. Vestweber, Nat. Rev. Immunol. **15**, 692 (2015).

[16] M. R. Prausnitz, S. Mitragotri, and R. Langer, Nat. Rev. Drug Discov. **3**, 115 (2004).

[17] T. Gratieri, I. Alberti, M. Lapteva, and Y. N. Kalia, Eur. J. Pharm. Sci. **50**, 609 (2013).

[18] X. Gao and F. C. Szoka, Acc. Chem. Res. **36**, 335 (2003).

[19] G. T. Linke, R. Lipowsky and T. Gruhn, Europhys. Lett. **74**, 916 (2006).

[20] G. Gompper and D. M. Kroll, Phys. Rev. E **52**, 4198 (1995).

[21] R. Lipowsky and E. Sackmann, *Structure and Dynamics of Membranes* (Elsevier Science, 1995).

[22] H. R. Shojaei and M. Muthukumar, J. Phys. Chem. B **120** 6102 (2016).

[23] M. Deserno and W. M. Gelbart, J. Phys. Chem. B **106** 5543 (2002).

[24] S. Salehyar and Q. Zhu, Soft Matter **12** 3156 (2016).

[25] W. E, W. Ren, and E. Vanden-Eijnden, Phys. Rev. B **66**, 052301 (2002).

[26] W. Ren, Commun. Math. Sci. **1**, 377 (2003).

[27] W. E, W. Ren, and E. Vanden-Eijnden, J. Chem. Phys. **126**, 164103 (2007).

[28] W. Ren and E. Vanden-Eijnden, J. Chem. Phys. **138**, 134105 (2013).

[29] P. Khunpetch, X. Man, T. Kawakatsu, and M. Doi, J. Chem. Phys. **148**, 134901 (2018).

[30] P. Walde, R. Wick, and M. Fresta, A. Annarosa Mangone, and P. L. Luisi, J. Am. Chem. Soc. **116**, 11649 (1994).

[31] R. Wick, P. Walde, and P. L. Luisi, J. Am. Chem. Soc. **117**, 1435 (1995).

[32] D. P. Cistola, J. A. Hamilton, and D. Jackson, Biochemistry **27**, 1881 (1988).

[33] T. F. Zhu and J. W. Szostak, J. Am. Chem. Soc. **131**, 5705 (2009).

[34] I. Budin, A. Debnath, and J. W. Szostak, J. Am. Chem. Soc. **134**, 20812 (2012).

[35] K. Takakura and T. Sugawara, Langmuir **20**, 3832 (2004).

[36] T. Toyota, K. Takakura, Y. Kageyama, K. Kurihara, N. Maru, K. Ohnuma, K. Kaneko, and T. Sugawara, Langmuir **24**, 3037 (2008).

[37] K. Kurihara, M. Tamura, K. Shoda, T. Toyota, K. Suzuki, and T. Sugawara, Nat. Chem. **3**, 775 (2011).

[38] Y. Sakuma and M. Imai, Phys. Rev. Lett. **107**, 198101 (2011).

[39] K. Emoto, T. Kobayashi, A. Yamaji, H. Aizawa, I. Tahara, K. Inoue, and M. Umeda, Proc. Natl. Acad. Sci. U.S.A. **93**, 12867 (1996).

[40] D. P. Siegel and M. M. Kozlov, Biophys. J. **87**, 366 (2004).

[41] T. Kaasgaard and C. J. Drummond, Phys. Chem. Chem. Phys. **8**, 4957 (2006).

[42] I. M. Hafez and P. R. Cullis, Adv. Drug Delivery Rev. **47**, 139 (2001).

[43] L. Onsager, Phys. Rev. **37**, 405 (1931).

[44] L. Onsager, Phys. Rev. **38**, 2265 (1931).

[45] M. Doi, *Soft Matter Physics* (Oxford University Press, Oxford, 2013).

[46] M. Doi, Chin. Phys. B **24**, 020505 (2015).

[47] M. Doi, J. Phys. Soc. Jpn. **78**, 052001 (2009).

[48] A. Onuki, *Phase Transition Dynamics* (Cambridge University Press, Cambridge, 2002).

[49] J. Happel and H. Brenner, *Low Reynolds Number Hydrodynamics* (Kluwer Academic Publishers, Dordrecht, 1963).

[50] A. Ulitsky and R. Elber, J. Chem. Phys. **92**, 1510 (1990).

[51] R. Olender and R. Elber, J. Chem. Phys. **105**, 9299 (1996).

[52] H. Jónsson, G. Mills, and K. W. Jacobsen, *Classical and Quantum Dynamics in Condensed Phase Simulations* (World Scientific, Singapore, 1998).

[53] P. Khunpetch, To be published in Thai J. Phys.

[54] G. E. Forsythe, M. A. Malcolm, and C. B. Moler, *Computer Methods for Mathematical Computations* (Prentice Hall, Englewood Cliffs, NJ, 1977).

[55] K. Müller and L. D. Brown, Theor. Chem. Acc. **53**, 75 (1979).

[56] L. D. Landau and E. M. Lifshitz, *Mechanics* (Butterworth-Heinemann, Oxford, 1982).

[57] K. Huang, *Statistical Mechanics* (John Wiley & Sons, New York, 1987).

[58] D. Marsh, Chem. Phys. Lipids **144**, 146 (2006).

[59] Rayleigh, Proc. Math. Soc. London **363**, 357 (1873).

[60] L. Onsager and S. Machlup, Phys. Rev. **91**, 6 (1953).

[61] L. Yu, M. Han, and F. He, Arabian J. Chem. (2013). (Article in Press)

[62] T. Darvishzadeh and N. V. Priezjev, J. Membr. Sci. **423**, 468 (2012).

[63] F. F. Nazzal and M. R. Wiesner, Water Environ. Res. **68**, 1187 (1996).

[64] W. Cumming, R. G. Holdich, and I. D. Smith, , J. Membr. Sci. **169**, 147 (2000).

[65] R. C. Baker, *An Introductory Guide to Flow Measurement*, (Professional Engineering Publishing, 2002).

[66] F. Peters and D. Arabali, Colloids and Surfaces A: Physicochem. Eng. Aspects, **426** 1 (2013).

APPENDICES

APPENDIX A

Derivation of the Vesicle's Evolution Equations from Onsager Variational Principle

In this appendix, we show the derivation of the vesicle's evolution equations from Onsager variational principle used in Chapter IV. The dynamics of the translocating vesicle can be described by a set of slow variables $\mathbf{x} = (r_1, r_2, n_1, n_2)$. However, we can reduce the degrees of freedom to two using the constraints $R_0^3 = r_1^3 + r_2^3$ and $N_0 = n_1 + n_2$. To make dynamics of the translocating vesicle clearer, we introduce two dimensionless variables x and y, defined by

$$x \equiv \left(\frac{r_1}{R_0}\right)^3, \tag{A.1}$$

and

$$y \equiv \frac{n_1}{N_0}, \tag{A.2}$$

respectively. The potential energy of the system can be written in terms of the two dimensionless variables as

$$\begin{aligned} A(x,y) &= a^2\lambda\Bigg\{2\pi\left(\frac{R_0}{a}\right)^2\left[\frac{(x^{2/3}-y)^2}{y} + \frac{((1-x)^{2/3}-(1-y))^2}{1-y}\right] \\ &\quad -\frac{4\pi}{3}\left(\frac{R_0}{a}\right)^3\left(\frac{\Delta P a}{\lambda}\right)(2x-1)\Bigg\}. \end{aligned} \tag{A.3}$$

In the limit of small Reynolds number, the dissipation function for the vesicle is given by

$$\begin{aligned}\Phi(\dot{x},\dot{y}) &= 8a^4\zeta_l\left(\frac{R_0}{a}\right)^4\Bigg\{\left(\frac{R_0}{3a}\right)^2\dot{x}^2+\left(1+\frac{\zeta_s}{\zeta_l a}\right)\frac{x^{4/3}(1-x)^{4/3}}{[(1-x)^{2/3}y+(1-y)x^{2/3}]^2}\dot{y}^2 \\ &\quad -\left(\frac{2R_0}{3a}\right)\frac{x^{2/3}(1-x)^{2/3}}{[(1-x)^{2/3}y+(1-y)x^{2/3}]}\dot{x}\dot{y}\Bigg\}. \end{aligned} \tag{A.4}$$

Next, we construct the Rayleighian of the system. Rayleighian is a sum of dissipation function and time derivative of the free energy. Then, the Rayleighian for the translocating vesicle is

$$R=\Phi+\dot{A}, \tag{A.5}$$

where Φ is given by Eq. (A.4) and $\dot{A}$ is given by

$$\begin{aligned}\dot{A} &= a^2\lambda\Bigg\{2\pi\left(\frac{R_0}{a}\right)^2\Bigg[\frac{2y(x^{2/3}-y)(\frac{2}{3}x^{-1/3}\dot{x}-\dot{y})-(x^{2/3}-y)^2\dot{y}}{y^2} \\ &\quad +\frac{2(1-y)((1-x)^{2/3}-(1-y))(-\frac{2}{3}(1-x)^{-1/3}\dot{x}+\dot{y})}{(1-y)^2} \\ &\quad +\frac{((1-x)^{2/3}-(1-y))^2\dot{y}}{(1-y)^2}\Bigg] \\ &\quad -\frac{8\pi}{3}\left(\frac{R_0}{a}\right)^3\left(\frac{\Delta P a}{\lambda}\right)\dot{x}\Bigg\}. \end{aligned} \tag{A.6}$$

The evolutions of x and y are determined by the condition that R is minimized with respect to $\dot{x}$ and $\dot{y}$, i.e. $\partial R/\partial\dot{x}=0$ and $\partial R/\partial\dot{y}=0$. This is the Onsager variational principle [43], [44], [45], [46]. Then, we obtain

$$\begin{aligned}\dot{x} &= -\frac{9}{16}\left(\frac{a^4\lambda}{R_0^6\zeta_l}\right)\left(1+\frac{\zeta_l a}{\zeta_s}\right)f(x,y) \\ &\quad -\frac{3}{16}\left(\frac{a^3\lambda}{R_0^5\zeta_l}\right)\left(\frac{\zeta_l a}{\zeta_s}\right)\left[\frac{y}{x^{2/3}}+\frac{(1-y)}{(1-x)^{2/3}}\right]g(x,y), \end{aligned} \tag{A.7}$$

and

$$\begin{aligned}\dot{y} &= -\frac{1}{16}\left(\frac{a^2\lambda}{R_0^4\zeta_l}\right)\left(\frac{\zeta_l a}{\zeta_s}\right)\left[\frac{y}{x^{2/3}}+\frac{(1-y)}{(1-x)^{2/3}}\right] \\ &\quad \left\{\left(\frac{3a}{R_0}\right)f(x,y)+\left[\frac{y}{x^{2/3}}+\frac{(1-y)}{(1-x)^{2/3}}\right]g(x,y)\right\}, \end{aligned} \tag{A.8}$$

where

$$f(x,y) = 2\pi\left(\frac{R_0}{a}\right)^2\left[\frac{4}{3}(x^{2/3}-y)\frac{x^{-1/3}}{y} - \frac{4}{3}((1-x)^{2/3}-(1-y))\frac{(1-x)^{-1/3}}{(1-y)}\right] - \frac{8\pi}{3}\left(\frac{R_0}{a}\right)^3\left(\frac{\Delta P a}{\lambda}\right), \tag{A.9}$$

and

$$g(x,y) = 2\pi\left(\frac{R_0}{a}\right)^2\left[-\frac{(x^{4/3}-y^2)}{y^2} + \frac{(1-x)^{4/3}-(1-y)^2}{(1-y)^2}\right]. \tag{A.10}$$

By introducing the dimensionless time $t' \equiv t/\tau$, where $\tau = \zeta_l a^3/2R_0\lambda$, we can rewrite $\dot{x}$ and $\dot{y}$ as

$$\dot{x} = \left(\frac{2R_0\lambda}{\zeta_l a^3}\right)\frac{dx}{dt'}, \tag{A.11}$$

and

$$\dot{y} = \left(\frac{2R_0\lambda}{\zeta_l a^3}\right)\frac{dy}{dt'}. \tag{A.12}$$

By substituting Eqs. (A.11) and (A.12) into Eqs. (A.7) and (A.8), respectively, we, finally, obtain the vesicle's evolution equations

$$\frac{dx}{dt'} = -\frac{9}{32}\left(\frac{a}{R_0}\right)^7\left(1+\frac{\zeta_l a}{\zeta_s}\right)f(x,y) - \frac{3}{32}\left(\frac{a}{R_0}\right)^6\left(\frac{\zeta_l a}{\zeta_s}\right)\left[\frac{y}{x^{2/3}} + \frac{(1-y)}{(1-x)^{2/3}}\right]g(x,y), \tag{A.13}$$

and

$$\frac{dy}{dt'} = -\frac{1}{32}\left(\frac{a}{R_0}\right)^5\left(\frac{\zeta_l a}{\zeta_s}\right)\left[\frac{y}{x^{2/3}} + \frac{(1-y)}{(1-x)^{2/3}}\right] \times\left\{\left(\frac{3a}{R_0}\right)f(x,y) + \left[\frac{y}{x^{2/3}} + \frac{(1-y)}{(1-x)^{2/3}}\right]g(x,y)\right\}. \tag{A.14}$$

APPENDIX B

Method of Volume of Solid of Revolution

Here, we will give a proof of the volume conservation inside the mother vesicle Eq. (5.12) by using the method of volume of solid of revolution.

In the birthing process, we have assumed that the daughter vesicle moves gradually and there is no water flowing out through the pore. Then, the water volume inside the mother vesicle is preserved. The situation is illustrated in Fig. B. 1.

We would like to calculate this constraint which is important for determining the variable R in terms of z_d in Chapter V. In order to calculate the change of the volume, we first need to find the volume inside of the mother vesicle which is the total volume of the mother vesicle subtracted by the volume of the daughter vesicle placed partially inside the mother vesicle, i.e.,

$$V' = \frac{4}{3}\pi R^3 - V_1 - V_2. \tag{B.1}$$

Let us introduce the method of volume of solid of revolution for calculating the volume of the daughter vesicle placed partially inside the mother vesicle, V_1 and V_2. The center of the daughter vesicle is located at point $(z_d, 0)$, where z_d is the distance between centers of the mother and daughter vesicles. Using the ansatz of Fig. B.1, the curve described the upper branch ($x > 0$) of the daughter vesicle is

$$x = \sqrt{b^2 - (z - z_d)^2}, \tag{B.2}$$

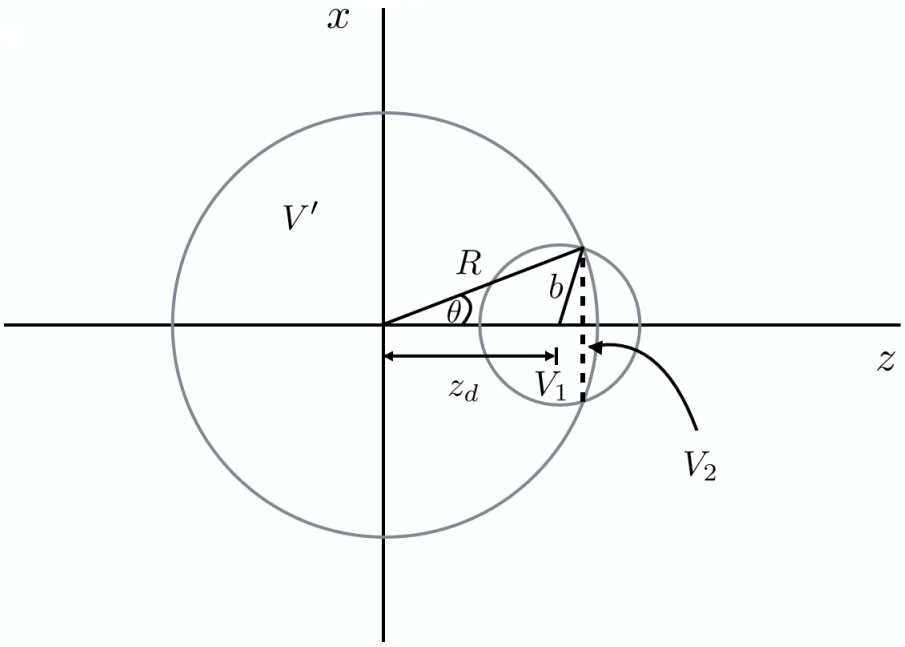

Figure B.1: The geometry of the daughter vesicle being expelled from the mother vesicle.

where b is radius of the rigid, spherical daughter vesicle. We then rotate this curve about z axis to get the surface of the solid of revolution which is the surface of the daughter vesicle. The volume of this object bounded by the interval $z \in [a, b]$ is given by

$$V = \int_a^b A(z)dz, \tag{B.3}$$

where $A(z)$ is the cross-sectional area of the solid.

To get the cross-sectional area, we cut the object perpendicular to the axis of rotation. The cross section is a solid disk with radius $x = \sqrt{b^2 - (z - z_d)^2}$. In this case, we get a solid disk with the area

$$\begin{aligned} A_1(z) &= \pi x^2 \\ &= \pi[b^2 - (z - z_d)^2]. \end{aligned} \tag{B.4}$$

This method is sometimes called the method of disks.

Then, the volume V_1 is easily obtained from the Eq. (B.3):

$$\begin{aligned} V_1 &= \pi \int_{z_d-b}^{R\cos\theta} [b^2 - (z - z_d)^2] dz \\ &= \pi b^2 (R\cos\theta - z_d + b) - \frac{\pi}{3}\Big[(R\cos\theta - z_d)^3 + b^3\Big]. \end{aligned} \tag{B.5}$$

Similarly, we can calculate V_2 from the same method. The mother vesicle is located at the origin and the curve described its upper branch ($x > 0$) is

$$x = \sqrt{R^2 - z^2}, \tag{B.6}$$

where R is radius of the mother vesicle. We again rotate the curve about z axis to get the surface of the mother vesicle. The cross-sectional area obtained by cutting the surface perpendicular to the z axis is

$$A_2(z) = \pi(R^2 - z^2). \tag{B.7}$$

Then, the volume V_2 is

$$\begin{aligned} V_2 &= \pi \int_{R\cos\theta}^{R} (R^2 - z^2) dz \\ &= \pi R^3 (1 - \cos\theta) - \frac{\pi}{3} R^3 (1 - \cos^3\theta). \end{aligned} \tag{B.8}$$

The total volume of the mother vesicle subtracted by the volume of the daughter vesicle placed partially inside the mother vesicle is

$$\begin{aligned} V' &= \frac{4}{3}\pi R^3 - V_1 - V_2 \\ &= \frac{4}{3}\pi R^3 - \pi b^2 (R\cos\theta - z_d + b) + \frac{\pi}{3}\Big[(R\cos\theta - z_d)^3 + b^3\Big] \\ &\quad -\pi R^3 (1 - \cos\theta) + \frac{\pi}{3} R^3 (1 - \cos^3\theta). \end{aligned} \tag{B.9}$$

Finally, the volume conservation is obtained as

$$\begin{aligned}
\Delta V &= V' - V_0 \\
&= \left\{ \frac{4}{3}\pi R^3 - \pi b^2 \Big[(R\cos\theta - z_d) + b \Big] \right. \\
&\quad + \frac{\pi}{3}\Big[(R\cos\theta - z_d)^3 + b^3 \Big] \\
&\quad \left. - \pi R^3 (1 - \cos\theta) + \frac{\pi R^3}{3}(1 - \cos^3\theta) \right\} \\
&\quad - \left\{ \frac{4}{3}\pi R_0^3 - \pi b^2 \Big[(R_0\cos\theta_0 - z_{d,0}) + b \Big] \right. \\
&\quad + \frac{\pi}{3}\Big[(R_0\cos\theta_0 - z_{d,0})^3 + b^3 \Big] \\
&\quad \left. - \pi R_0^3 (1 - \cos\theta_0) + \frac{\pi R_0^3}{3}(1 - \cos^3\theta_0) \right\} \\
&= 0, \qquad \text{(B.10)}
\end{aligned}$$

where V_0 is the total volume of the mother vesicle subtracted by the volume of the daughter vesicle placed partially inside the mother vesicle at the initial state.